

AD \_\_\_\_\_

Award Number: W81XWH-11-1-0608

TITLE: Genetically Engineered Mouse Model of Diffuse Intrinsic Pontine Glioma as a Preclinical Tool

PRINCIPAL INVESTIGATOR: Oren Becher, MD

CONTRACTING ORGANIZATION: Duke University  
Durham, NC 27705

REPORT DATE: November 2014

TYPE OF REPORT: Final

PREPARED FOR: U.S. Army Medical Research and Materiel Command  
Fort Detrick, Maryland 21702-5012

DISTRIBUTION STATEMENT: Approved for Public Release;  
Distribution Unlimited

The views, opinions and/or findings contained in this report are those of the author(s) and should not be construed as an official Department of the Army position, policy or decision unless so designated by other documentation.

<b>REPORT DOCUMENTATION PAGE</b>				<i>Form Approved</i> <b>OMB No. 0704-0188</b>	
Public reporting burden for this collection of information is estimated to average 1 hour per response, including the time for reviewing instructions, searching existing data sources, gathering and maintaining the data needed, and completing and reviewing this collection of information. Send comments regarding this burden estimate or any other aspect of this collection of information, including suggestions for reducing this burden to Department of Defense, Washington Headquarters Services, Directorate for Information Operations and Reports (0704-0188), 1215 Jefferson Davis Highway, Suite 1204, Arlington, VA 22202-4302. Respondents should be aware that notwithstanding any other provision of law, no person shall be subject to any penalty for failing to comply with a collection of information if it does not display a currently valid OMB control number. <b>PLEASE DO NOT RETURN YOUR FORM TO THE ABOVE ADDRESS.</b>					
<b>1. REPORT DATE</b> November 2014		<b>2. REPORT TYPE</b> Final		<b>3. DATES COVERED</b> 1 Sep 2011 - 31 Aug 2014	
<b>4. TITLE AND SUBTITLE</b> Genetically Engineered Mouse Model of Diffuse Intrinsic Pontine Glioma as a Preclinical Tool				<b>5a. CONTRACT NUMBER</b>	
				<b>5b. GRANT NUMBER</b> W81XWH-11-1-0608	
				<b>5c. PROGRAM ELEMENT NUMBER</b>	
<b>6. AUTHOR(S)</b> Oren Becher MD  E-Mail: oren.becher@duke.edu				<b>5d. PROJECT NUMBER</b>	
				<b>5e. TASK NUMBER</b>	
				<b>5f. WORK UNIT NUMBER</b>	
<b>7. PERFORMING ORGANIZATION NAME(S) AND ADDRESS(ES)</b>  Duke University 450 Research Drive, LSRC B362 Durham, NC 27710				<b>8. PERFORMING ORGANIZATION REPORT NUMBER</b>	
<b>9. SPONSORING / MONITORING AGENCY NAME(S) AND ADDRESS(ES)</b> U.S. Army Medical Research and Materiel Command Fort Detrick, Maryland 21702-5012				<b>10. SPONSOR/MONITOR'S ACRONYM(S)</b>	
				<b>11. SPONSOR/MONITOR'S REPORT NUMBER(S)</b>	
<b>12. DISTRIBUTION / AVAILABILITY STATEMENT</b> Approved for Public Release; Distribution Unlimited					
<b>13. SUPPLEMENTARY NOTES</b>					
<b>14. ABSTRACT</b> Diffuse Intrinsic Pontine Gliomas or DIPG, is a type of brain tumor that afflicts children and is the leading cause of death in pediatric brain tumor patients. One major obstacle to progress has been the lack of representative animal models that recapitulate the genetic alterations of the human disease in the appropriate cell-of-origin. Recent analysis of human DIPGs have unraveled the following key genetic alterations: K27M H3.3 or H3.1 mutations in 80% of tumors, p53 mutations in 75% of tumors, and focal amplification of components of the RTK/Ras/PI3K pathway in approximately 50% of tumors with 30% of tumors harboring amplification of PDGFR $\alpha$ . Using the RCAS/tv-a system, we have previously reported the development of a DIPG model by overexpression of PDGF-B in nestin progenitors of Ink4a-ARF deficient mice. Here we report the development of several improved DIPG models by overexpression of PDGF-B and Cre in nestin progenitors of conditional p53 deficient mice, conditional PTEN mice, and combined conditional p53 and PTEN mice. In addition we have also generated a new DIPG model by overexpression of PDGF-B and Cre in GFAP progenitors of conditional p53 mice. Using expression profiling we note that they are genetically distinct. Lastly, to identify unique aspects of brainstem gliomagenesis we have compared the expression profile of the above described murine DIPG model to cortical gliomas induced by the same genetic alterations and unraveled that pax3 is a differentially expressed transcription factor that is upregulated in DIPGs and not in cortical gliomas.					
<b>15. SUBJECT TERMS</b> nothing listed					
<b>16. SECURITY CLASSIFICATION OF:</b>			<b>17. LIMITATION OF ABSTRACT</b>  UU	<b>18. NUMBER OF PAGES</b>  39	<b>19a. NAME OF RESPONSIBLE PERSON</b> USAMRMC
<b>a. REPORT</b> U	<b>b. ABSTRACT</b> U	<b>c. THIS PAGE</b> U			<b>19b. TELEPHONE NUMBER</b> (include area code)

## Table of Contents

	<u>Page</u>
Introduction.....	2
Overall Project Summary.....	3
Key Research Accomplishments.....	13
Reportable Outcomes.....	13
Conclusion.....	14
References.....	14
Appendices.....	15

## Introduction

Brain tumors are currently the leading cause of death for children with cancer. Diffuse Intrinsic Pontine Gliomas or DIPG, is a type of brain tumor that afflicts children and is the leading cause of death in pediatric brain tumor patients. One major obstacle to progress has been the lack of representative animal models that recapitulate the genetic alterations of the human disease in the appropriate cell-of-origin. Recent analysis of human DIPGs have unraveled the following key genetic alterations: K27M H3.3 or H3.1 mutations in 80% of tumors, p53 mutations in 75% of tumors, and focal amplification of components of the RTK/Ras/PI3K pathway in approximately 50% of tumors with 30% of tumors harboring amplification of PDGFR $\alpha$  (1-5). Using the RCAS/tv-a system, we have previously reported the development of a DIPG model by overexpression of PDGF-B in nestin progenitors of Ink4a-ARF deficient mice. Here we report the development of several improved DIPG models by overexpression of PDGF-B and Cre in nestin progenitors of conditional p53 deficient mice, conditional PTEN mice, and combined conditional p53 and PTEN mice. In addition we have also generated a new DIPG model by overexpression of PDGF-B and Cre in GFAP progenitors of conditional p53 mice. Principle component analysis of the expression profiles of these DIPG mouse models demonstrates that they are genetically distinct. Lastly, to identify unique aspects of brainstem gliomagenesis we have compared the expression profile of the above described murine DIPG model to cortical gliomas induced by the same genetic alterations and unraveled that pax3 is a differentially expressed transcription factor that is upregulated in DIPGs and not in cortical gliomas. In year 2, we have analyzed whether H3.3K27M is sufficient to drive gliomagenesis (with or without p53 loss) and observed the formation of ectopic proliferating cell clusters but no tumors. In addition, we have also identified c-myc as a differentially expressed gene between the PDGF-B; p53 deficient model and the PDGF-B; PTEN deficient model. In year 3 we used our most improved DIPG model (PDGF-B; H3.3K27M; and p53 loss) as a preclinical tool to help prioritize the translation of novel agents for clinical trials for children with DIPG. We evaluated the antitumor activity of two of the top hits from an *in vitro* drug screen performed as part of the DIPG preclinical consortium (Panobinostat, and BMS754807). Short-term treatment with Panobinostat did not significantly inhibit proliferation or induce apoptosis and a week treatment with BMS 754807 did not significantly prolong survival. Our analysis suggests that the lack of efficacy of BMS-754807 is due to poor drug penetration across the blood-brain-barrier. A similar analysis is ongoing for panobinostat.

## Key Words:

DIPG= Diffuse Intrinsic Pontine Glioma (A fatal type of brain cancer that arises in children)

PDGF-B= Platelet Derived Growth Factor-B (a growth factor that is used to develop the DIPG mouse model)

K27M H3.3/H3.1= a recently discovered mutation in Histone 3.3 or Histone 3.1 that is present in 80% of DIPGs.

RCAS/tv-a system= an avian retroviral system used to deliver growth factors or mutant genes to cells in the mouse brain.

Panobinostat= a new type of cancer drug targeting histone deacetylase enzymes

BMS 754807= a new type of cancer drug targeting IGF-1R

P53 loss= p53 is a tumor suppressor that is commonly inactivated in DIPGs.

## Overall Project Summary

Below are results on the specific tasks as described in the Statement of Work:

### Task 1-Develop improved DIPG (Diffuse Intrinsic Pontine Glioma) mouse models that recapitulate human DIPG genetic alterations

**Task 1a-** Infect the ventricular system of the posterior fossa of Nestin Tv-a; p53<sup>fl/fl</sup> (floxed/floxed) neonatal mice with RCAS-PDGF-B (Replication-Competent, Avian leukemia virus [ALV] long terminal repeat [LTR], Splice acceptor- Platelet-derived growth factor- B) and RCAS-Cre (20 mice per group)

This task has been completely successfully. We have generated these tumors and an example of one is illustrated in Figure 1. Out of 54 nestin tv-a; p53 floxed mice that were infected with PDGF and Cre, 46 developed murine DIPGs (85% success rate). Hydrocephalus mice were excluded from this calculation. With this particular experiment the hydrocephalus rate is 57% (due to the formation of leptomeningeal tumor). Figure 1 compares the tumor latency from Task 1a and Task 2c. Tumors formed in Task 1a are significantly more aggressive than tumors formed in Task 2c. Please note that we are including more than 20 mice per group in this survival analysis to demonstrate the difference between the two models. The additional tumor-bearing mice are not part of this award.

Figure 1

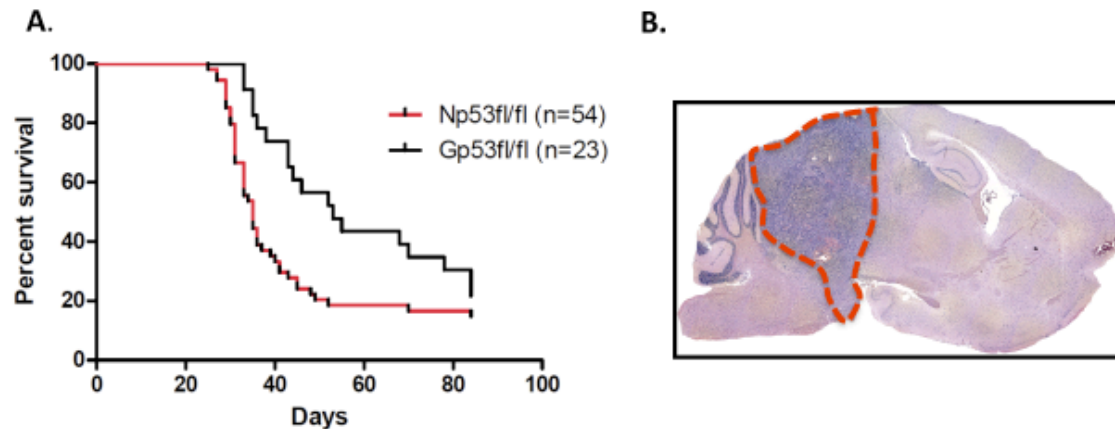


**Figure 1** A. Survival curves comparing tumor latency in the Nestin tv-a p53 floxed model and GFAP tv-a p53 floxed model. Log Rank test demonstrates that overexpression of PDGF-B with Cre in nestin progenitors results in more aggressive DIPGs with shorter latency ( $p=0.019$ ) B. Low magnification image of a DIPG induced in Nestin tv-a; p53 floxed mice. Red dotted line marks the tumor boundary.

**Task 1b-** Infect the ventricular system of the posterior fossa of Nestin Tv-a; PTEN<sup>fl/fl</sup> neonatal mice with RCAS-PDGF-B and RCAS-Cre (20 mice per group)

This task is completed. We have generated 10 tumors and an example of one is described in the figure below. Hydrocephalus mice were excluded from the analysis. The hydrocephalus rate was 51% for this experiment due to the formation of leptomeningeal tumor.

**Figure 2**

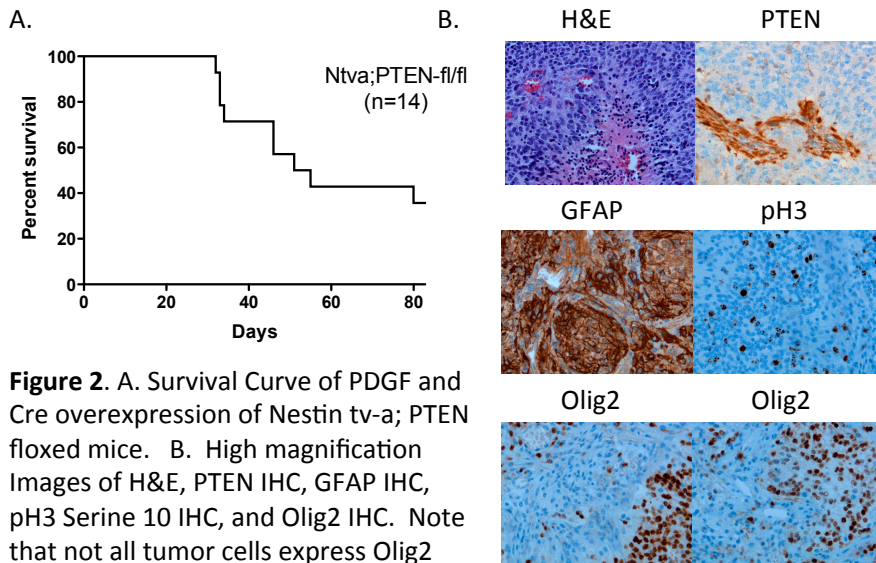
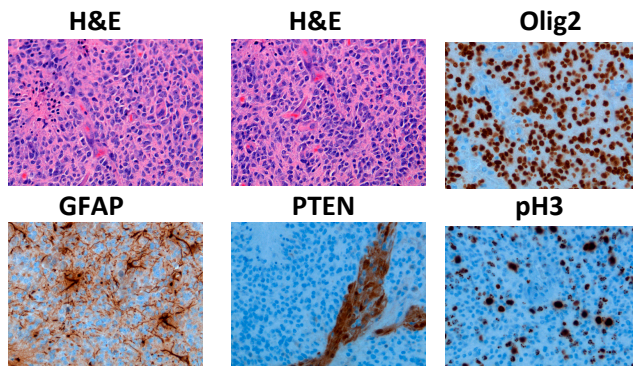


**Figure 2.** A. Survival Curve of PDGF and Cre overexpression of Nestin tv-a; PTEN floxed mice. B. High magnification Images of H&E, PTEN IHC, GFAP IHC, pH3 Serine 10 IHC, and Olig2 IHC. Note that not all tumor cells express Olig2

**Task 1c-** Infect the ventricular system of the posterior fossa of Nestin Tv-a; p53<sup>fl/fl</sup>; PTEN<sup>fl/fl</sup> neonatal mice with RCAS-PDGF-B and RCAS-Cre (20 mice per group)

**This task has been completed. We have generated six such tumors and an example of one is described below (Figure 3). Hydrocephalus mice were excluded from the analysis. The hydrocephalus rate for this experiment was 63% (due to the formation of leptomenigeal tumor).**

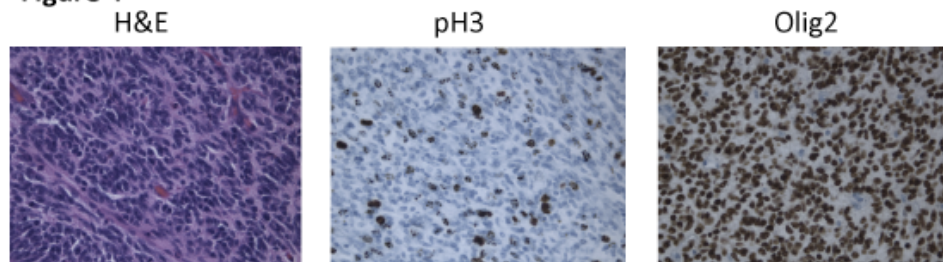
**Figure 3**



**Figure 3.** Representative H&Es and IHC for Olig2, pH3 (Serine 10), PTEN, GFAP. Note that PTEN staining is only present in the tumor vasculature

**Task 1d-** Analyze three tumors per genotype above by IHC (immunohistochemistry) for Ki-67, Cleaved caspase 3, GFAP (Glial Fibrillary Acidic Protein), nestin, Olig-2, SMA (Smooth Muscle Actin), and CD31.

**This task is completed. Representative IHC for task 1b and 1c are illustrated in Figure 2 and 3 respectively. We have successfully immunostained for cleaved caspase 3 in year 2. CD31 IHC was performed in year 3. For task 1a, representative IHC are in Figure 4 and Figure 8.**

**Figure 4**

**Figure 4.** Representative H&E, pH3 Serine 10, and Olig2 of a PDGF; p53 deficient DIPG induced in nestin tv-a; p53 floxed mice.

**Task 1E-** Perform expression profiling of PDGF-B driven DIPG tumors of all the genotypes above (10 tumors per group)

We have performed RNA seq of 3 PDGF; p53 deficient tumors (from nestin tv-a mice), 3 PDGF; p53 deficient; PTEN deficient tumors, 3 PDGF; PTEN deficient tumors, and PDGF; p53 deficient tumors (from GFAP tv-a mice). There were significant differentially expressed genes between the different DIPG genotypes. The three tables below lists the top 10 significant differentially expressed genes of the distinct DIPG genotypes relative to the PDGF-B; p53 deficient model (from nestin tv-a mice). Note that Myc was one of the significantly differentially expressed genes between PDGF-B; p53 deficient model and the PDGF-B; PTEN deficient model (we confirmed this finding by RT PCR and immunofluorescence). In addition, each genotype clusters separately using principle component analysis (see figure 5).

**Table 1**

**Top 10 significantly differentially expressed genes of murine DIPGs driven by PDGF-B and p53 loss vs. PDGF-B and combined p53 loss and PTEN loss**

Gene Name	Nestin.p53.mean	Nestin.p53.PTEN.mean	Fold change	padj
Gm5506	33.4	3496.1	104.7	4.8E-300
Gm11847	15.3	1155.8	75.7	6.0E-150
Gm13699	318.9	1181.6	3.71	3.54E-28
Sycp1	4.0	162.2	40.03	1.47E-23
Tecta	213.7	719.4	3.37	1.26E-17
6820431F20Rik	4709.5	9023.1	1.92	2.87E-14
Gm16103	1.85	88.3	47.6	5.19E-13
Meg3	14288.7	7845	0.55	9.28E-13
Mmp14	3028	6837.7	2.26	1.42E-11
Capn6	466.3	1304	2.80	8.49E-11

**Table 2**

**Top 10 significant differentially expressed genes of murine DIPGs driven by PDGF-B and p53 loss vs. PDGF-B and PTEN loss**

Gene Name	Nestin.p53.mean	Nestin.PTEN.mean	Fold change	padj
Plxnb3	5940.1	1077.2	0.18	9.42E-32
RP23-381B19.7.1	872.4	100.9	0.12	2.11E-31
Igf2bp2	657.6	65.8	0.1	2.59E-24
Srpk3	643.6	99.65	0.15	1.69E-20
Gm3435	242.9	1118.3	4.6	8.65E-20
<b>Myc</b>	<b>3084</b>	<b>870.5</b>	<b>0.28</b>	<b>1.17E-19</b>

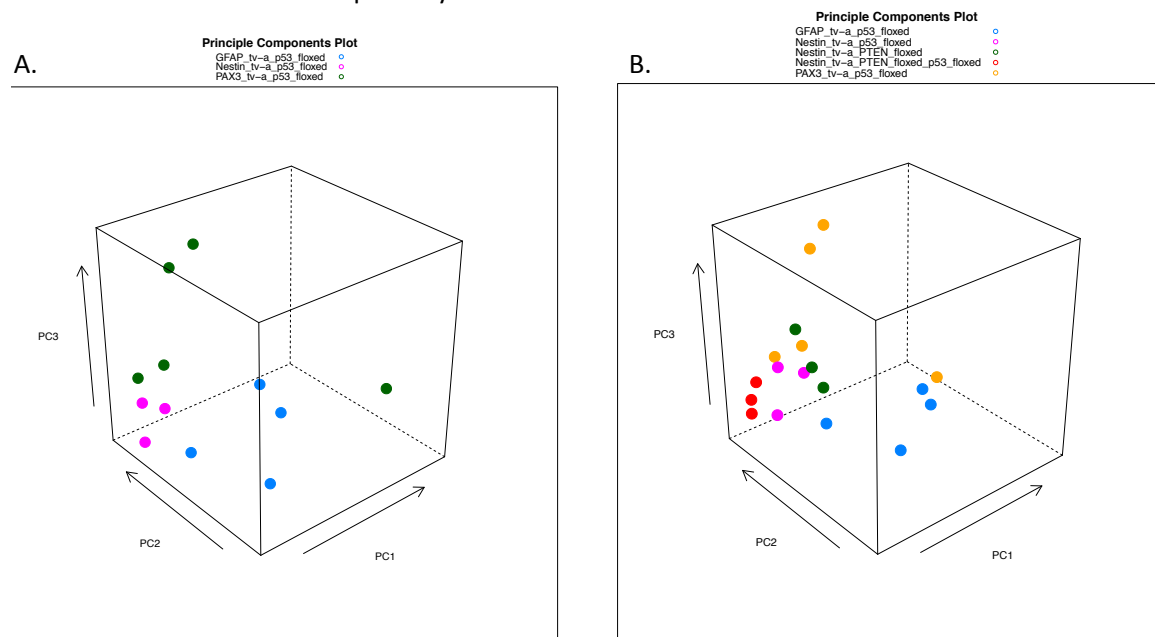
9030025P20Rik	60.8	448.1	7.37	4.54E-17
Celf5	559.8	1879.9	3.36	1.59E-15
Sym	775.2	2421.9	3.12	4.36E-15
Pcdhb3	459.1	1558.9	3.396	9.37E-15

**Table 3**

**Top 10 significantly differentially expressed genes between PDGF-B; p53 deficient murine DIPGs induced by infection of Nestin progenitors vs. GFAP progenitors**

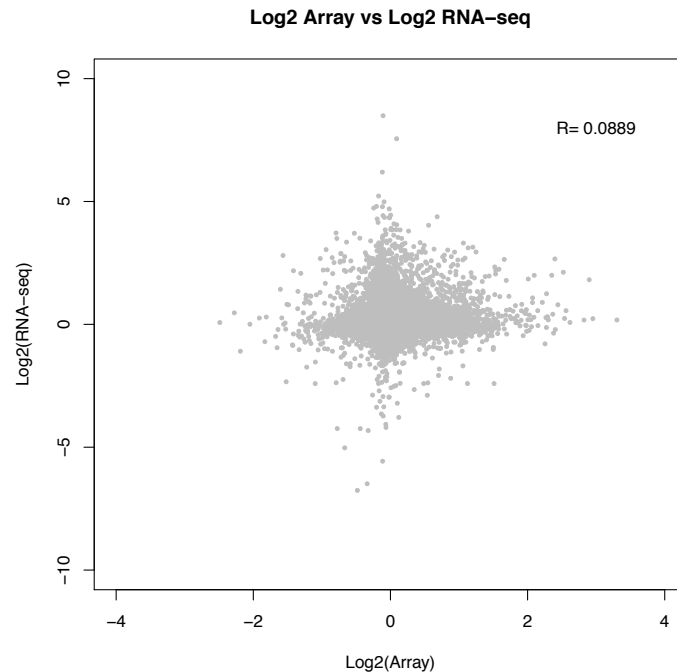
Gene Name	Nestin.p53.mean	GFAP.p53.mean	Fold change	padj
Gm5514	86.3	1.67	0.0194	5.13E-12
Gm8730	426.2	2331.4	5.47	1.7E-08
Gm9625	292.4	1793.5	6.13	8.2E-08
Mrpl48-ps	126.8	7.51	0.06	5.99E-07
Gm14165	10.64	242.9	22.8	2.79E-05
Tubb3	6577.1	2067.7	0.314	0.0003
Samd9l	1677.9	414.6	0.247	0.0003
Parp12	2530.6	762.9	0.301	0.0005
Gm5806	5.64	396.9	70.4	0.0006
Gm7658	286.5	63.9	0.222	0.0009

Figure 5. A. Murine DIPGs induced with PDGF and p53 loss in distinct cells-of-origin cluster separately with principle component analysis. B. Murine DIPGs induced with distinct driver combinations also cluster separately.



**Task 1F-** Compare (in consultation with the DNA Microarray Facility at Duke) the differentially expressed genes between PDGF-B; H3.3K27M; p53 loss and PDGF-B; p53 loss to the differentially expressed genes between human DIPGs with H3.3K27M to human DIPGs without histone mutations.

Task completed. Please see below (correlation was relative low  $R=0.0889$ ) which can be related to the fact that the human tumors are more heterogeneous.



**Task 1G-** Infect the ventricular system of the posterior fossa of Ntv-a (Nestin tv-a) with RCAS-H3.3 K27M and Ntv-a; p53 floxed mice with RCAS-H3.3 K27M + RCAS-Cre (20 mice per group).

**We infected 8 Ntv-a mice with H3.3 K27M and observed the mice for tumor formation. None of the mice developed symptoms of brain tumor formation and so at 12 weeks post infection, mice were euthanized, brains extracted, fixed in formalin, and embedded in paraffin. H&E analysis demonstrated that no tumors formed. We immunostained the brain sections for HA (as the H3.3K27M construct was HA tagged) and observed rare HA positive cells. There were rare proliferating cells that were HA negative. In addition, we infected 20 Ntv-a; p53 floxed mice with H3.3K27M and Cre and observed the mice for tumor formation. Although the majority of the mice did not develop symptoms of brain tumor formation, we observed the presence of ectopic proliferating clusters of tumor cells in 72% of the mice. This was recently published in Science (Lewis et al. Science 2013).**

**Below is a representative image of a proliferating ectopic cell cluster (Figure 6).**

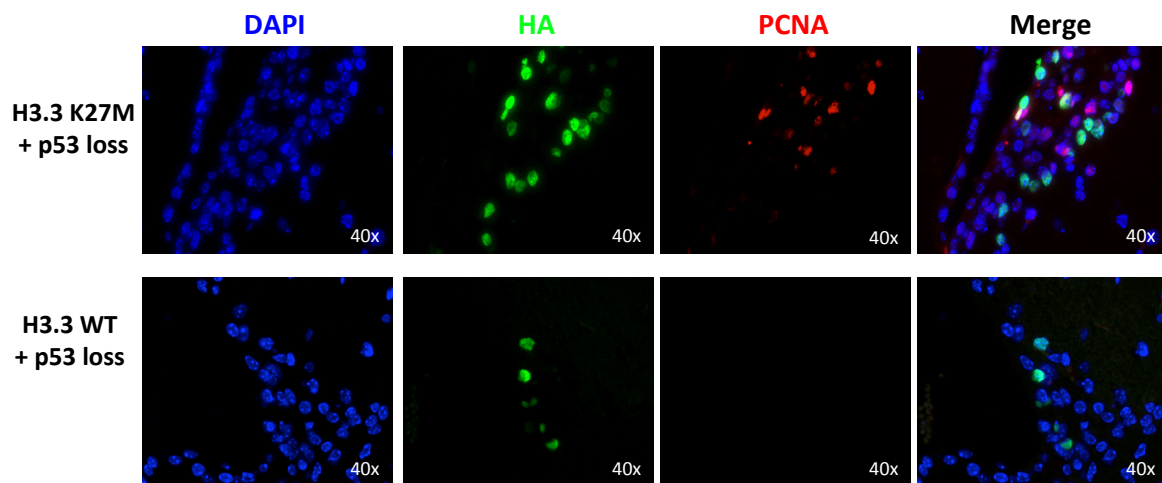


**Figure 6- Proliferating ectopic cell clusters but no tumor formation with K27M H3.3 expression + p53 loss in the postnatal murine brainstem**  
A. High magnification (40X) double immunofluorescence for HA (K27M) and PCNA demonstrating an ectopic cell cluster containing K27M-positive cells and PCNA-positive cells. B. High magnification (40X) double immunofluorescence for HA (H3.3 WT) and PCNA demonstrating the absence of PCNA-positive cells around H3.3 WT-positive cells.

## **Task 2 – Investigate potential cells-of-origin and developmental window for DIPG formation**

**Task 2a -** Infect the ventricular system of the posterior fossa of GFAP tv-a neonatal mice (20 mice) with RCAS-PDGF-B and observe for development of tumors

**This task has been completed.** We have generated twelve tumors so far and a representative H&E of GFAP tv-a (Gtv-a) tumor is illustrated in Figure 7 (next to an H&E of a Ntv-a tumor which is quite similar histologically). Hydrocephalus mice have been excluded from the analysis. Percent hydrocephalus for this experiment was 50%, which was due to leptomeningeal tumor.

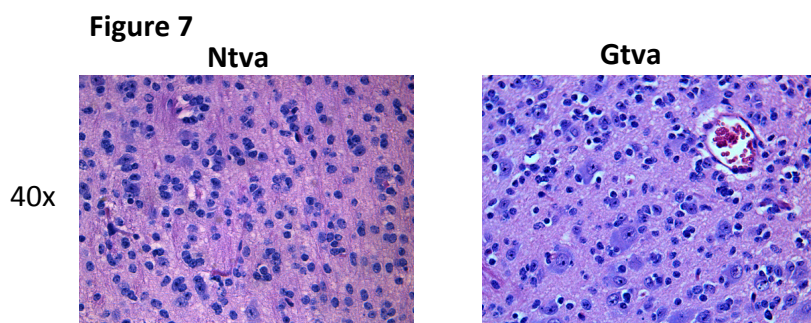


**Figure 7-** High magnification H&E of PDGF induced low-grade brainstem gliomas In Ntv-a and Gtv-a mice.

**Task 2b -** infect the ventricular system of the posterior fossa of GFAP-tv-a; p53<sup>fl/fl</sup> neonatal mice with RCAS H3.3 K27M together with RCAS-Cre and observe for the development of tumors (20 mice)

**This task is complete.** We injected 6 mice with H3.3K27M and Cre and we did not observe the formation of tumors. We did observe the formation of ectopic clusters in a subset of

the mice similar to our observations in Task 1G. We also injected 9 mice with H3.3 K27M alone. No tumors were formed.

**Task 2c** - Infect the ventricular system of the posterior fossa of GFAP-tv-a; p53<sup>fl/fl</sup> neonatal mice (20 mice) with RCAS-PDGF-B together with RCAS-Cre and observe for development of tumors

This task has been completed and the survival curve for this mouse cohort was included in Figure 1. Out of 23 GFAP tv-a; p53 floxed mice infected with RCAS-PDGF-B and RCAS-Cre, 18 developed gliomas (78% success rate).

**Immunohistochemical characterization relative to**

Nestin tv-a model p53 floxed model is illustrated in Figure 8 (no significant differences in H&E or immunostaining for GFAP or nestin). Hydrocephalus mice were excluded from the analysis. The hydrocephalus rate for this experiment was 56% (due to leptomenigeal tumor).

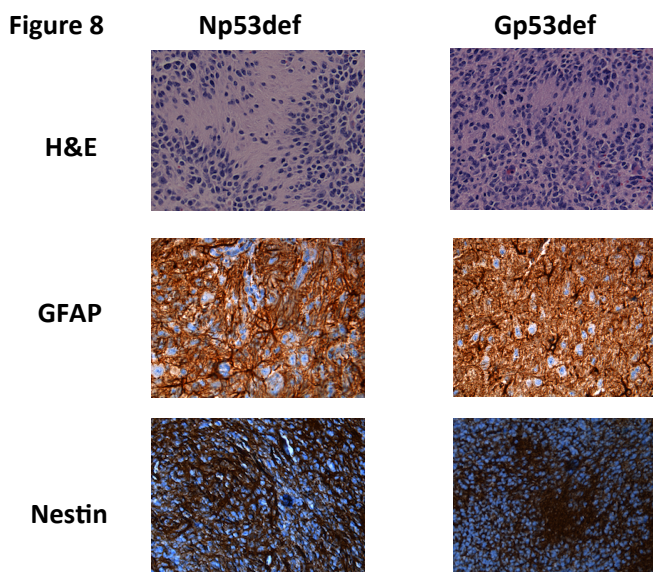


Figure 8. Murine DIPGs induced by PDGF-B and p53 loss in two distinct cells-of-origin: Nestin and GFAP are indistinguishable by H&E or immunostaining for nestin or GFAP.

**Task 2d** - Infect the ventricular system of the posterior fossa of Ntv-a; p53<sup>fl/fl</sup> neonatal mice with RCAS- PDGF-B and RCAS-Cre at postnatal D2, postnatal D7, and postnatal D14 (20 mice per group).

This task is completed. Our results for the postnatal D7 injections were that 10 mice developed tumors. Our results for the postnatal D14 injections were that 6 mice developed tumors. By H&E, the tumors look similar to the tumors induced at D2.

**Task 2e**- Perform expression profiling of PDGF-B cortical tumors (5 tumors) and compare to results from task 1E in consultation with the DNA Microarray facility at Duke.

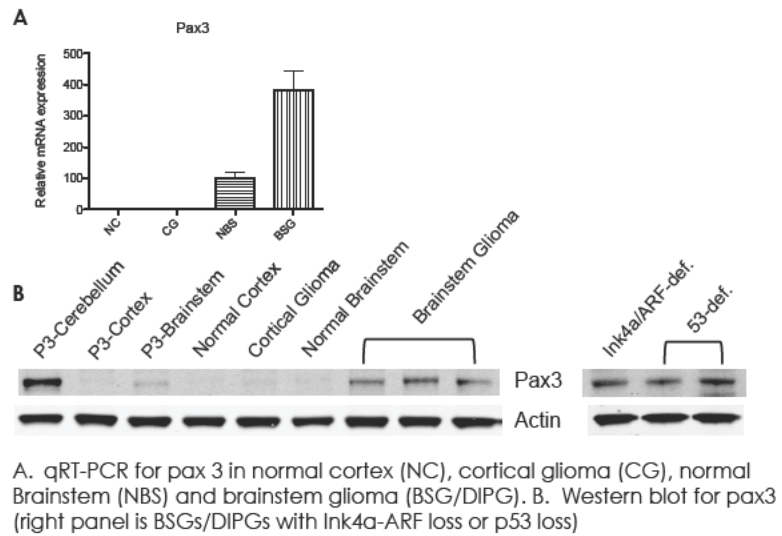
This task has been completed. Our results identified Pax3 as a differentially expressed gene between brainstem gliomas (BSGs=DIPG) and cortical gliomas. We performed expression

Gene	Fold change BSG vs. NBS	P-value BSG vs. NBS	Fold Change BSG vs. CG	P-Value BSG vs. CG
Etl4	-17.3	1.67E-08	-3.20	1.65E-05
Slc22a3	11.61	3.63E-08	3.56	5.89E-06
Bmp4	-2.57	3.47E-07	-2.77	1.94E-07
Chl1	-7.21	2.66E-06	-12.9	3.66E-07
Pax3	4.96	1.04E-05	8.44	1.20E-06
Irx5	3.34	0.00267	19.0	6.15E-06
Pcyt1b	2.49	1.11E-05	2.46	1.24E-05
Myo5b	-2.41	0.00553	-7.59	2.41E-05
Ubt1	1.97	2.30E-05	2.01	1.86E-05

profiling of murine brainstem and murine cortical gliomas, induced by overexpressing PDGF-B in nestin expressing progenitors in the brainstem or cortex respectively of Ntv-a;Ink4a-ARF deficient mice. To our surprise, there were only 9 genes that were significantly differentially expressed between brainstem gliomas (BSG=DIPG) and cortical gliomas (CG) and significantly differentially regulated between normal brainstem (NBS) and BSG (table on the left). In this short list, we chose to focus on pax3; a transcription factor that is known to have oncogenic functions in neural crest

derived tissues, and has already been implicated in having region-specific expression in ependymoma and pilocytic astrocytoma. Pax3 belongs to the paired box family of transcription factors. It is known to have regionalized expression in the developing neural tube and to confer positional identity to neural precursors (dorsal-ventral axis). Its expression and role in brainstem gliomagenesis are not known. Recently, Pax3 has been shown to inversely correlate with GFAP expression, a marker of differentiation in the astrocytic lineage. We confirmed that *pax3* mRNA is overexpressed in brainstem gliomas by real time RT PCR and also observed that Pax3 protein is overexpressed in brainstem gliomas relative to normal brainstem and cortical gliomas (Figure 7). We also confirmed that this region-specific expression of *pax3* is in the tumor compartment by using Olig2-GFP mice. By sorting DIPG tumor cells in the Olig2-GFP background for GFP, we sorted for the tumor cell compartment and observed that *pax3* mRNA is mostly expressed in Olig-2 expressing tumor cells (data not shown).

Figure 9



**Task 3- Evaluate the efficacy of immunotoxins alone and in combination with targeted agents that are administered by direct or systemic delivery to treat PDGF-B induced DIPGs. Each treatment group will have a similarly sized group of vehicle or sham treated mice with similar sized tumors (MRI (Magnetic Resonance Imaging or MRI will be used to measure tumor size)**

With regards to Tasks related to Aim 3, we made the following three changes in year 3:

- 1. Use PDGF-B; H3.3K27M; p53 deficient model instead of PDGF-B; p53 deficient model-** initially when we submitted the grant in 2010, it was not yet known that the majority of DIPGs have H3.3/H3.1 K27M mutations. In addition, as PDGFR $\alpha$  amplifications co-occur with H3.3K27M mutations (4), we have proceeded to develop a PDGF-B; H3.3K27M; p53 deficient model (Lewis et al., 2013) which used in Task 3 in replacement of the PDGF-B; p53 deficient model.
- 2. Update drugs that are more likely to be translated into a clinical trial for children with DIPG.** As part of the DIPG preclinical consortium (where cell-lines from the above-developed models were used in a drug screen together with human DIPG cell-lines), we have identified new drugs that may be more efficacious (and in addition, some of the drugs proposed in 2010 such as perifosine, and temsirolimus have already been shown to have limited efficacy in children with DIPG) and so we made changes to our task list (total mice number will stay the same).
- 3. Focus on systemic delivery as opposed to both systemic and direct delivery (CED).** We have tried CED with CP868, 596 (a PDGFR $\alpha$  inhibitor) in four tumor-bearing mice but have not seen any hint of efficacy. In addition, this approach is very challenging in our model as our model is very aggressive. Lastly, CED requires MRI before and after treatment and is very costly. So we feel that we would make more translational advances by focusing on systemic delivery.

**Task 3b-** Generate PDGF-induced DIPG mice as in **Task 1a** (10 mice per group) and treat with CP868,596 (a PDGFR $\alpha$  inhibitor from AROG (AROG pharmaceuticals)) via (a) systemic delivery using an osmotic pump placed subcutaneously for 5 days (this drug has a 30 min half-life in mice) as well as (b) direct delivery via CED (as described in **Task 3a**). Analysis of the treatment response as in **Task 3a**.

Systemic analysis of CP868, 596 via osmotic pump did not demonstrate any efficacy. The graph below (Figure 10) is quantification of pH3 Serine 10 of five drug-treated mice and five vehicle-treated mice. We have also treated 6 tumor-bearing mice with CED (four with drug and two with vehicle) but did not observe any significant change in proliferation as assessed by pH3 Serine 10 (Figure 11). Given the complexity of CED where there are numerous variables to control such as drug concentration, volume, length of infusion, we prefer to focus on evaluating drugs by systemic delivery.

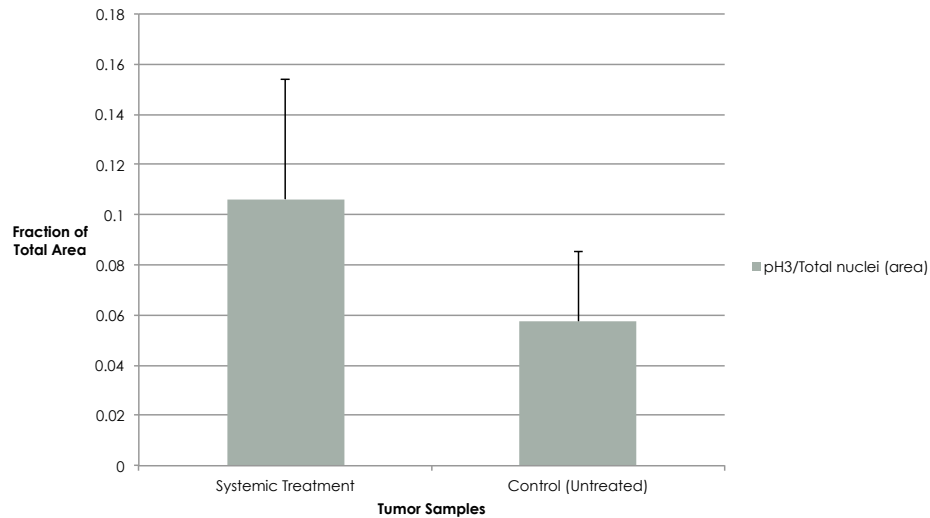


**Figure 10.** Systemic treatment with crenolanib (CP868,596) via osmotic pump does not decrease the proliferation rate of the tumors. The treatment group comprised of 5 mice and the vehicle group also comprised of 5 mice.

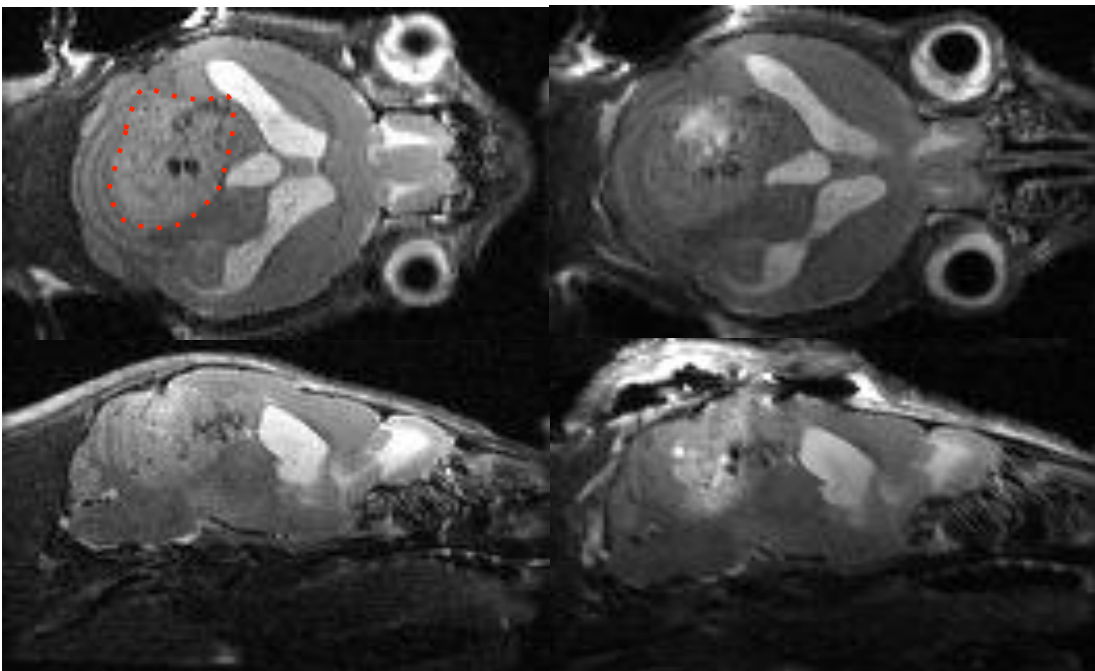


**Figure 11.** MRI Images on the left are axial and sagittal MRI images pre-convection enhanced delivery infusion of crenolanib. Images on the right are post-convection enhanced delivery. Crenolanib was co-infused with gadolinium (notice the increase in contrast in images on the right). Tumor area is demarcated in top left image (in red).

**Task 3c-** Generate PDGF-induced DIPG mice driven by PDGF; H3.3K27M; p53 loss (described in Lewis et al., 2013) and treat with BMS-754807 at 25mg/kg IP BID for 3-5 days (10 mice per group: drug vs. vehicle). Analysis of treatment response as in Task 3a.

Task completed (This task was done with PDGF-B; p53 deficient mice). We observed no significant change in proliferation as measured by pH3 and a very modest but significant increase in apoptosis as measured with cleaved caspase 3 with treatment with BMS-754807.

**Task 3d-** Generate PDGF-induced DIPG mice driven by PDGF; H3.3K27M; p53 loss (described in Lewis et al., 2013) and treat with panobinostat 10mg/kg IP for 5 days (10 mice per group: drug vs. vehicle). Analysis of treatment response as in Task 3a.

Task completed and results are below (Figure 12). Basically, Panobinostat did not significantly inhibit proliferation (measured with phosphoH3) or induce apoptosis (measured with Cleaved Caspase 3)

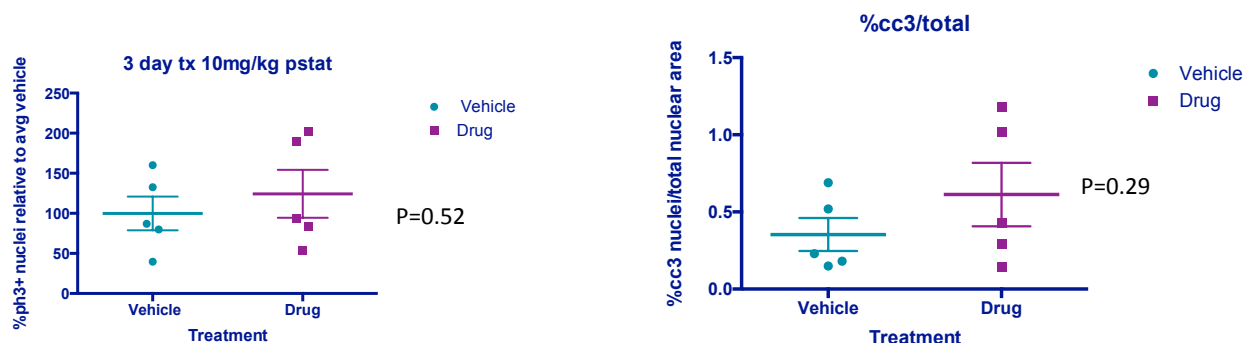


Figure 12. Short-term treatment with panobinostat does not significantly impact tumor cell proliferation or apoptosis of the PDGF-B; H3.3K27M;p53 deficient model

**Task 3e-** Generate PDGF-induced DIPG mice driven by PDGF-B; H3.3K27M; p53 loss and treat with BMS-754807 in combination with panobinostat (10 mice per group: drugs vs. vehicles). Analysis of treatment response as in Task 3a.

This task was modified slightly and instead of testing the combination, we thought it would be more meaningful from a translational standpoint to better understand why neither drug worked as a single agent. So we treated tumor-bearing mice with BMS-754807 alone, Panobinostat alone, or vehicle for either drug and collected tumor tissue to measure drug level in the tumor tissue. The results demonstrate that not enough BMS-754807 gets across the blood-brain-barrier to the tumor (concentration in the tumor is below the IC50 of the drug *in vitro*). Panobinostat analysis is pending but samples have been collected.

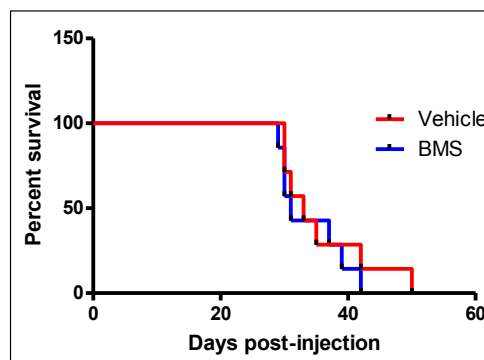


Figure 13. Treatment of PDGF-B; H3.3K27M; p53 deficient tumor-bearing mice with BMS 754807 does not significantly prolong survival.

**Task 3f-** Survival analysis will be carried out with the most promising agent or combination based on results from **Task 3a, 3b, 3c, 3d, 3e** (10 mice per group).

As we had short-term data that BMS 754807 significantly induced apoptosis in the PDGF-B; p53 deficient model, we hypothesized that BMS 754807 would prolong survival in the PDGF-B; H3.3K27M; p53 deficient model. However, BMS 754807 did not significantly prolong survival (Figure 13). Preliminary analysis of the mechanism of resistance suggests limited drug delivery across the blood-brain-barrier and will be the subject of future studies.

### Key Research Accomplishments

1. The establishment of improved DIPG animal models that can be used as preclinical tools. Each of these models has a unique genetic profile as evident by a principle component analysis.
2. We have observed that GFAP expressing cells in the brainstem can also be transformed to generate DIPGs.
3. We have generated cell-lines from the genetically engineered DIPG models that are being used as part of the DIPG preclinical consortium (together with several laboratories that are using human DIPG xenografts) to help prioritize the translation of novel agents for clinical trials for children with DIPG.
4. The identification of pax3 as a significantly differentially expressed gene between cortical gliomas and brainstem gliomas (DIPGs) that are driven by the same genetic alterations (PDGF and Ink4-ARF loss). This transcription factor is significantly upregulated in 40% of human DIPGs (a subset that is older at presentation, has PDGFRA and cell cycle amplifications, and is ACVR1 wild type). These results suggest that there may be two subtypes of human DIPGs. This was recently published.
5. We observed that although expression of H3.3K27M with p53 loss in neonatal brainstem progenitors is not sufficient to induce gliomas, it results in the expression of ectopic proliferating clusters suggestive of pre-neoplastic lesions. These findings were published. Our best model at the moment (which recapitulates the genetic alterations of the human disease) includes PDGF-B; H3.3K27M; p53 loss.
6. C-myc is differentially expressed between the PDGF-B; p53 deficient model and the PDGF-B; PTEN deficient model (both generated in nestin tv-a mice) and will be studied in the future.
7. BMS754807 and panobinostat are examples of two drugs that demonstrate efficacy *in vitro* but not *in vivo*, highlighting the challenge of drug delivery for brain cancer.

**No inventions, patents or licenses filed.**

### REPORTABLE OUTCOMES

1. We published two manuscripts from this DOD award. The published pax3 work was also presented in ISPNO 2012 as a poster and at SNO 2014 as an oral presentation.

Lewis PW, Müller MM, Koletsky MS, Cordero F, Lin S, Banaszynski LA, Garcia BA, Muir T, **Becher OJ**, Allis CD. (2013) Inhibition of PRC2 activity by gain-of-function H3 mutations found in pediatric glioblastoma. *Science*, 340(6134): 857-61. PMID: 23539183. (<http://www.ncbi.nlm.nih.gov/pubmed/?term=23539183>)

Misuraca KL, Barton KL, Chung A, Diaz AK, Conway S, Corcoran DL, Baker SJ, and **Becher OJ**. (2014) Pax3 Expression Enhances PDGF-B-Induced Brainstem Gliomagenesis and Characterizes a Subset of Brainstem Glioma. *Acta Neuropathologica Communications*. 2014 2(1): 134. PMCID: PMC4210596

2. DIPG mouse models that recapitulate the genetic alterations of the human disease
  - A. PDGF B; p53 deficient DIPG with nestin progenitors as cells-of-origin
  - B. PDGF B; PTEN deficient DIPG with nestin progenitors as cells-of-origin
  - C. PDGF B; p53 and PTEN deficient DIPG with nestin progenitors as cells-of-origin
  - D. PDGF B; p53 deficient DIPG with GFAP progenitors as cells-of-origin

2. Expression profiling of the above models revealed significant differentially expressed genes. Intriguingly, C-myc is a differentially expressed gene between the PDGF B; PTEN deficient DIPG model and the PDGF; p53 deficient DIPG model.
3. Results from this grant served as preliminary data for a Damon Runyon Clinical Investigator Award application (based on results from task 2E) titled **Region-specific differences in CNS Gliomagenesis**, which was successful.
4. We have generated cell-lines derived from our models, which are being used as part of the DIPG preclinical consortium, and/or being shared with other researchers.

## Conclusion

Diffuse Intrinsic Pontine Glioma is an incurable tumor in 2014. This tumor is the leading cause of death in children with brain tumors. Our laboratory is one of few laboratories around the world that is studying this rare incurable tumor. Our approach is unique as we are using genetic engineered mouse modeling techniques to dissect the contribution of specific drivers to brainstem gliomagenesis, to identify the cell(s)-of-origin for DIPG formation, and to develop improved DIPG mouse models as preclinical tools. Our accomplishments as part of this award are as follows: the development of improved DIPG mouse models, including a DIPG mouse model with a potentially different cell-of-origin marker (GFAP as opposed to Nestin). In addition, we have identified pax3 as a transcription factor that identifies a subset of the human disease. In year three of the award, we focused on preclinical testing with our most improved DIPG mouse model driven by PDGF-B; H3.3K27M; p53 loss and chose to evaluate BMS-754807 or Panobinostat, two drugs that came up as promising agents for DIPG in an *in vitro* drug screen. However, thus far we have not observed significant anti-tumor activity *in vivo* with these two agents, which may be related to drug delivery. This is something that we will follow-up on in subsequent studies.

## References:

1. Wu et al. Somatic histone H3 alterations in pediatric diffuse intrinsic pontine gliomas and nonbrainstem glioblastomas. *Nat Genet* 2012; 44:251–253
2. Schwartzentruber J, et al. Driver mutations in histone H3.3 and chromatin remodeling genes in paediatric glioblastoma. *Nature* 2012 482:226–231
3. Grill J et al. Critical oncogenic mutations in newly diagnosed pediatric diffuse intrinsic pontine glioma. *Pediatr Blood Cancer* 2012 58:489-91
4. Khuong-Quang DA et al. K27M mutation in histone H3.3 defines clinically and biologically distinct subgroups of pediatric diffuse intrinsic pontine gliomas. *Acta Neuropathol* 2012; 124:439-47
5. Puget S. et al. 2012. Mesenchymal Transition and PDGFRA Amplification/Mutation Are Key Distinct Oncogenic Events in Pediatric Diffuse Intrinsic Pontine Gliomas. *PLoS One* 2012; 7:e30313
6. Lewis PW, et al. 2013. Inhibition of PRC2 activity by gain-of-function H3 mutations found in pediatric glioblastoma. *Science*, 340(6134): 857-61. PMID: 23539183.



## Inhibition of PRC2 Activity by a Gain-of-Function H3 Mutation Found in Pediatric Glioblastoma

Peter W. Lewis *et al.*

*Science* **340**, 857 (2013);

DOI: 10.1126/science.1232245

*This copy is for your personal, non-commercial use only.*

If you wish to distribute this article to others, you can order high-quality copies for your colleagues, clients, or customers by [clicking here](#).

Permission to republish or repurpose articles or portions of articles can be obtained by following the guidelines [here](#).

**The following resources related to this article are available online at [www.sciencemag.org](http://www.sciencemag.org) (this information is current as of May 20, 2013 ):**

**Updated information and services**, including high-resolution figures, can be found in the online version of this article at:

<http://www.sciencemag.org/content/340/6134/857.full.html>

**Supporting Online Material** can be found at:

<http://www.sciencemag.org/content/suppl/2013/03/27/science.1232245.DC1.html>

A list of selected additional articles on the Science Web sites **related to this article** can be found at:

<http://www.sciencemag.org/content/340/6134/857.full.html#related>

This article **cites 14 articles**, 7 of which can be accessed free:

<http://www.sciencemag.org/content/340/6134/857.full.html#ref-list-1>

This article has been **cited by** 1 articles hosted by HighWire Press; see:

<http://www.sciencemag.org/content/340/6134/857.full.html#related-urls>

This article appears in the following **subject collections**:

Medicine, Diseases

<http://www.sciencemag.org/cgi/collection/medicine>

Molecular Biology

[http://www.sciencemag.org/cgi/collection/molec\\_biol](http://www.sciencemag.org/cgi/collection/molec_biol)

We instead suggest that most previous assessments have overestimated global mass losses because of the interpolation of sparse glaciological measurements that are not representative for the largest glacierized regions. We can only demonstrate this negative bias for the 2003–2009 period, but it has long been suspected for earlier periods as well (34, 35). This calls for a reexamination of previous global estimates based on the interpolation of glaciological records, which will probably lead to a downward revision of the estimated total contribution of glaciers to sea level rise over the past century.

Our consensus estimate of glacier mass wastage between 2003 and 2009 implies a sea-level contribution of  $0.71 \pm 0.08$  mm of sea-level equivalent (SLE) year<sup>-1</sup>, accounting for  $29 \pm 13\%$  of the observed sea-level rise ( $2.50 \pm 0.54$  mm year<sup>-1</sup>) for the same period (11). The total glacier mass loss is comparable to a recent estimate for the whole of Greenland and Antarctica (36) (peripheral glaciers + ice sheets) for the period 2003–2008. To avoid double counting, we subtracted our estimates for peripheral glacier mass loss from this total to obtain a total ice-sheet mass budget of  $-290 \pm 50$  Gt year<sup>-1</sup> (11) and a total land ice (all glaciers + ice sheets) mass budget of  $-549 \pm 57$  Gt year<sup>-1</sup>, amounting to a sea-level rise of  $1.51 \pm 0.16$  mm of SLE year<sup>-1</sup>, which is  $61 \pm 19\%$  of the total global sea-level rise (11).

#### References and Notes

1. M. F. Meier *et al.*, *Science* **317**, 1064 (2007).
2. J. G. Cogley, *Ann. Glaciol.* **50**, 96 (2009).
3. G. Kaser, J. G. Cogley, M. B. Dyurgerov, M. F. Meier, A. Ohmura, *Geophys. Res. Lett.* **33**, L19501 (2006).
4. T. Jacob, J. Wahr, W. T. Pfeffer, S. Swenson, *Nature* **482**, 514 (2012).
5. J. A. Church *et al.*, *Geophys. Res. Lett.* **38**, L18601 (2011).
6. A. Arendt *et al.*, *Randolph Glacier Inventory: A Dataset of Global Glacier Outlines Version: 2.0* (Global Land Ice Measurements from Space, Digital Media, Boulder, CO, 2012).
7. M. Zemp, M. Hoelzle, W. Haeberli, *Ann. Glaciol.* **50**, 101 (2009).
8. G. Moholdt, C. Nuth, J. O. Hagen, J. Kohler, *Remote Sens. Environ.* **114**, 2756 (2010).
9. I. Sasgen, V. Klemann, Z. Martinec, *J. Geodyn.* **59–60**, 49 (2012).
10. S. B. Luthcke, A. A. Arendt, D. D. Rowlands, J. J. McCarthy, C. F. Larsen, *J. Glaciol.* **54**, 767 (2008).
11. Materials and methods are available in the supplementary materials on Science Online.
12. B. Wouters, D. Chambers, E. J. O. Schrama, *Geophys. Res. Lett.* **35**, L20501 (2008).
13. A. S. Gardner *et al.*, *Nature* **473**, 357 (2011).
14. G. Moholdt, B. Wouters, A. S. Gardner, *Geophys. Res. Lett.* **39**, L10502 (2012).
15. A. Bliss, R. Hock, J. G. Cogley, *Ann. Glaciol.* **54**, 191 (2013).
16. P. Rastner *et al.*, *Cryosphere* **6**, 1483 (2012).
17. H. D. Pritchard *et al.*, *Nature* **484**, 502 (2012).
18. S. R. M. Ligtenberg, M. M. Helsen, M. R. van den Broeke, *Cryosphere* **5**, 809 (2011).
19. R. Hock, M. de Woul, V. Radic, M. Dyurgerov, *Geophys. Res. Lett.* **36**, L07501 (2009).
20. E. J. Rinne *et al.*, *J. Geophys. Res.* **116**, F03024 (2011).
21. T. Bolch *et al.*, *Geophys. Res. Lett.* **40**, 875 (2013).
22. T. Bolch *et al.*, *Science* **336**, 310 (2012).
23. A. Kääb, E. Berthier, C. Nuth, J. Gardelle, Y. Arnaud, *Nature* **488**, 495 (2012).
24. J. Gardelle, E. Berthier, Y. Arnaud, *Nat. Geosci.* **5**, 322 (2012).
25. E. R. Ivins *et al.*, *J. Geophys. Res.* **116**, B02403 (2011).
26. M. J. Willis, A. K. Melkonian, M. E. Pritchard, J. M. Ramage, *Remote Sens. Environ.* **117**, 184 (2012).
27. M. J. Willis, A. K. Melkonian, M. E. Pritchard, A. Rivera, *Geophys. Res. Lett.* **39**, L17501 (2012).
28. A. K. Melkonian *et al.*, *Cryosphere Discuss.* **6**, 3503 (2012).
29. E. Schiefer, B. Menounos, R. Wheate, *Geophys. Res. Lett.* **34**, L16503 (2007).
30. M. Dyurgerov, M. F. Meier, R. L. Armstrong, *Mass Balance of Mountain and Sub-Polar Glaciers Outside the Greenland and Antarctic ice sheets: Supplement to*

*Occasional Paper No. 55* (Institute of Arctic and Alpine Research, University of Colorado, Boulder, CO, 2005).

31. E. Berthier, E. Schiefer, G. K. C. Clarke, B. Menounos, F. Remy, *Nat. Geosci.* **3**, 92 (2010).
32. E. Rignot, A. Rivera, G. Casassa, *Science* **302**, 434 (2003).
33. A. S. Gardner, G. Moholdt, A. Arendt, B. Wouters, *Cryosphere* **6**, 1103 (2012).
34. M. B. Dyurgerov, M. F. Meier, *Arct. Alp. Res.* **29**, 379 (1997).
35. J. G. Cogley, W. P. Adams, *J. Glaciol.* **44**, 315 (1998).
36. A. Shepherd *et al.*, *Science* **338**, 1183 (2012).

**Acknowledgments:** We thank K. Matsuo, M. Huss, T. Jacob, A. Kääb, S. Luthcke, A. Willsman, M. Willis, and I. Sasgen for updated or early access to regional estimates of glacier mass change; M. Flanner, T. Jacob, and S. Swenson for helping with analysis of the hydrologic models; A. Bliss, N. Mölg, C. Nuth, P. Rastner, M. Willis, and G. Wolken for providing regional areas of ocean-terminating glacier basins; J. Lenaerts and J. van Angelen for providing RACMO2 output for Greenland and Antarctica; J. Box and C. Chen for making available Greenland Ice Sheet snowline estimates; G. A. R. Riva, and P. Stocchi for providing glacial isostatic adjustment models; and C. Starr and the NASA/Goddard Space Flight Center Scientific Visualization Studio for help with Fig. 1. This work was supported by funding to A.S.G. and M.J.S. from the Natural Sciences and Engineering Research Council of Canada, G.M. from NASA award NNX09AE52G, B.W. from a Marie Curie International Outgoing Fellowship within the 7th European Community Framework Programme (FP7-PEOPLE-2011-IOF-301260), E.B. from the TOSCA program of the French Space Agency (CNES), R.H. from NASA grants NNX11AF41G and NNX11A023G and NSF grant ANT-1043649, G.K. from Austrian Science Fund (FWF) grant P25362-N26, T.B. from the Deutsche Forschungsgemeinschaft (DFG, BO 3199/2-1), and F.P. from European Space Agency project Glaciers\_cci (4000101778/10/1-AM).

#### Supplementary Materials

www.sciencemag.org/cgi/content/full/340/6134/852/DC1  
Materials and Methods  
Figs. S1 to S10  
Tables S1 to S5  
References

26 December 2012; accepted 7 March 2013  
10.1126/science.1234532

## Inhibition of PRC2 Activity by a Gain-of-Function H3 Mutation Found in Pediatric Glioblastoma

Peter W. Lewis,<sup>1</sup> Manuel M. Müller,<sup>2</sup> Matthew S. Koletsky,<sup>1</sup> Francisco Cordero,<sup>3</sup> Shu Lin,<sup>4</sup> Laura A. Banaszynski,<sup>1</sup> Benjamin A. Garcia,<sup>4</sup> Tom W. Muir,<sup>2</sup> Oren J. Becher,<sup>3</sup> C. David Allis<sup>1\*</sup>

Sequencing of pediatric gliomas has identified missense mutations Lys27Met (K27M) and Gly34Arg/Val (G34R/V) in genes encoding histone H3.3 (*H3F3A*) and H3.1 (*HIST3H1B*). We report that human diffuse intrinsic pontine gliomas (DIPGs) containing the K27M mutation display significantly lower overall amounts of H3 with trimethylated lysine 27 (H3K27me3) and that histone H3K27M transgenes are sufficient to reduce the amounts of H3K27me3 in vitro and in vivo. We find that H3K27M inhibits the enzymatic activity of the Polycomb repressive complex 2 through interaction with the EZH2 subunit. In addition, transgenes containing lysine-to-methionine substitutions at other known methylated lysines (H3K9 and H3K36) are sufficient to cause specific reduction in methylation through inhibition of SET-domain enzymes. We propose that K-to-M substitutions may represent a mechanism to alter epigenetic states in a variety of pathologies.

Somatic mutations in genes encoding proteins that modify chromatin dynamics frequently contribute to tumorigenesis (1). Mutations in subunits of the Polycomb repressive complex 2 (PRC2) are often associated with tu-

mor progression (2). PRC2 normally helps maintain epigenetic gene silencing and X chromosome inactivation through enzymatic di- and trimethylation of K27 on histone H3 (3). In addition to enzymatic machinery, histone H3 missense mu-

tations in pediatric gliomas represent direct evidence that alterations of the histones themselves can promote cancer. In two pediatric brain cancers, diffuse intrinsic pontine gliomas (DIPGs) and supratentorial glioblastoma multiforme (GBMs), 60% of patients studied exhibited one of two mutually exclusive mutations in either *H3F3A*, one of two genes encoding the histone H3 variant H3.3, or *HIST3H1B*, one of several genes encoding H3.1 (4–6). The K27M mutation occurring in either *H3F3A* or *HIST3H1B* was observed in nearly 80% of DIPGs, and 22% of non-brain stem gliomas (6).

We sought to determine whether DIPG samples that contain the K27M mutation exhibit global changes in key regulatory histone modifications. Immunoblots with antisera raised against the K27M substitution (fig. S1A) indicated the presence of

<sup>1</sup>Laboratory of Chromatin Biology and Epigenetics, The Rockefeller University, New York, NY 10065, USA. <sup>2</sup>Department of Chemistry, Princeton University, Princeton, NJ 08544, USA.

<sup>3</sup>Departments of Pediatrics and Pathology, Preston Robert Tisch Brain Tumor Center, Duke University Medical Center, Durham, NC 27710, USA. <sup>4</sup>Department of Biochemistry and Biophysics, Perelman School of Medicine, University of Pennsylvania, Philadelphia, PA 19104, USA.

\*Corresponding author. E-mail: alliscd@rockefeller.edu

H3 K27M protein in DIPG samples containing *H3F3A* (H3.3) or *HIST3H1B* (H3.1) alleles (Fig. 1A). DIPG tumors containing H3K27M mutations exhibited both a decrease in H3 with trimethylated lysine 27 (H3K27me3) and a modest increase in amounts of H3 with acetylated lysine 27 (H3K27ac) by immunoblot with modification-specific antisera (Fig. 1, A and C). Quantification of H3K27me3 by immunohistochemistry demonstrated that K27M mutant DIPGs contained significantly less H3K27me3 than non-K27M mutant DIPGs (Fig. 1D). The H3.1/3 K27M protein is 3.63% ( $\pm 0.33$ ) to 17.61% ( $\pm 1.11$ ) of total H3 in human DIPG samples, as measured by quantitative mass spectrometry (fig. S1B). Two histone modifications related to transcription and/or activation (H3K4me3 and H3K36me3) were similar in DIPG samples regardless of tumor genotype, which could be used to argue that global changes in posttranslational modifications were specific to H3K27. Using a platelet-derived growth factor (PDGF)-induced brain stem glioma model to characterize this mutation in vivo (7), we found that transgenic H3.3K27M was sufficient to increase H3K27ac and to significantly reduce H3K27me3 (Fig. 1, B to D). Expression of H3.3K27M with p53 loss in nestin progenitors of the neonatal mouse brain stem was not sufficient to generate gliomas but did induce proliferating ectopic cell clusters in 72% (21

out of 29) of the mice (fig. S1C), whereas expression of the wild-type H3.3 with p53 loss ( $n = 8$ ) in nestin progenitors of the neonatal mouse brain stem did not result in the induction of ectopic proliferating cell clusters (fig. S1D).

To investigate the mechanism by which H3K27M decreased overall H3K27me3, we generated stable human embryonic kidney–293T (HEK293T) cell lines that express FLAG- and hemagglutinin (HA) epitope-tagged wild-type histone H3.3 or K27M and G34R/V mutants, which contributed to about 1% of total cellular histone H3, as measured by immunoblot. Cells expressing the H3K27M mutant histone exhibited a profound reduction in H3K27me2/3, with little changes in the amounts of H3K4me3 or H3K36me3 (Fig. 2A). This reduction was specific to the H3K27M mutation, as amounts of H3K27me2/3 remained unchanged in H3.3G34R/V transgenic cell lines. We did not observe change in the amounts of PRC2 complex components in H3.3K27M, PDGF-induced glioblastoma cell lines (fig. S2A).

The heterozygous and invariant nature of the lysine-to-methionine mutation at residue 27 in nearly 80% of pediatric DIPGs strongly suggests that this specific amino acid substitution imparts a unique gain-of-function to the mutant histone. To further test the specificity of this substitution, we performed a

survey of all amino acid substitutions at H3K27. Nearly all substitutions had little effect, if any, on the amounts of K27me3, with the exception of methionine, and to a lesser extent isoleucine (Fig. 2B).

The global reduction in H3K27me2/3 suggested that the H3K27M transgene reduced methylation on endogenous wild-type H3 histones. Indeed, purified heterotypic mononucleosomes (1:1 ratio of H3.3-FLAG-HA: endogenous H3.3), oligonucleosomes containing H3K27M, or wild-type oligonucleosomes from K27M-expressing cells displayed a marked decrease in H3K27me3 on the endogenous H3 protein (fig. S2B). Concomitantly, these nucleosomes exhibited a modest increase in the acetylation of H3K27 (H3K27ac) on the untagged H3 in the heterotypic K27M nucleosomes (Fig. 2C), and, similar to the modification pattern observed on mononucleosomes, oligonucleosome arrays showed elevated H3K27ac when they contained H3.3K27M (Fig. 2D).

We investigated amounts of H3K36me3 in cell lines carrying H3.3G34R/V mutations to determine whether these mutations behave similarly to H3K27M. Although overall amounts of H3K36me3 remained unchanged in H3.3G34R/V cell lines, a marked loss of H3K36me3 was exclusive to the epitope-tagged H3.2/3 of purified mono- or oligonucleosomes (Fig. 2, B and C). The epitope-

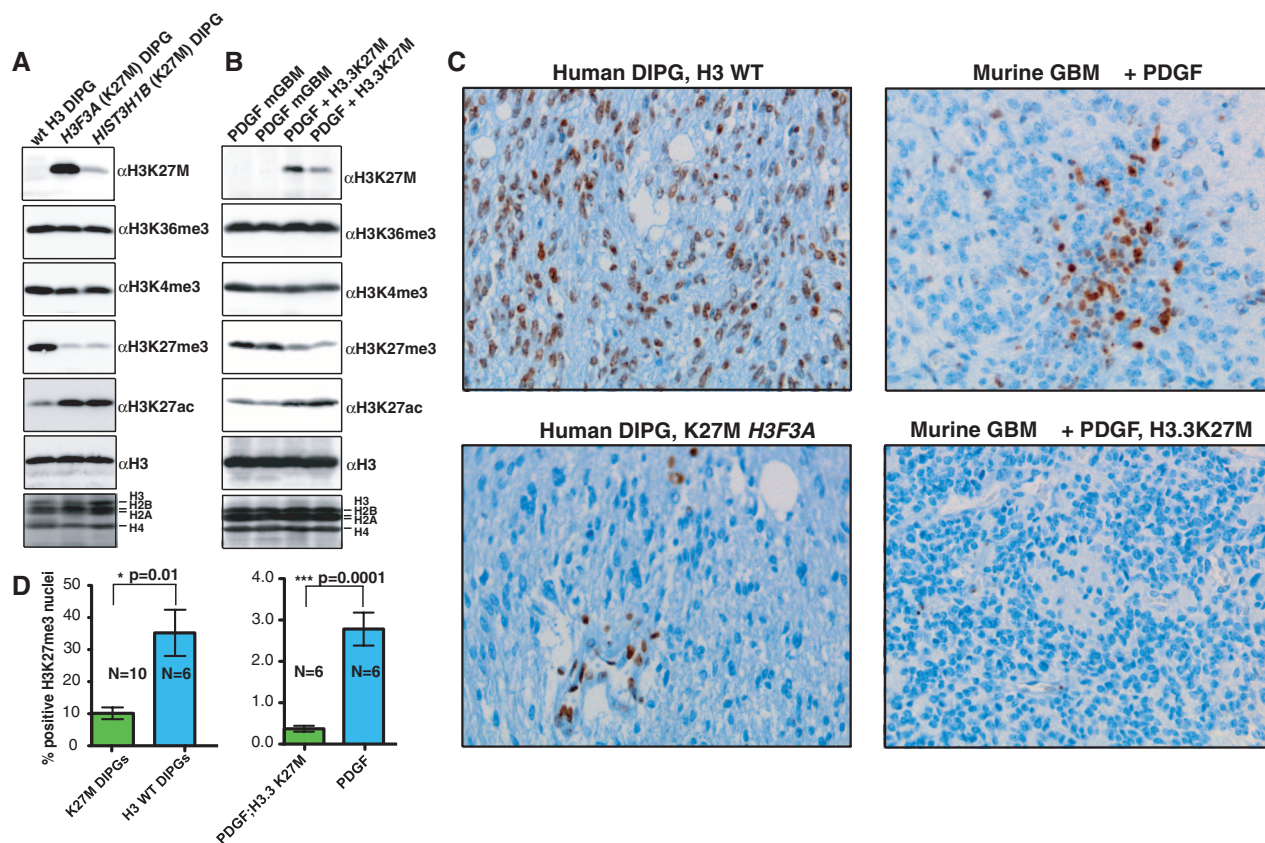


**Fig. 1. Histones extracted from human DIPG containing *H3F3A* K27M (H3.3) or *HIST3H1B* K27M (H3.1) mutations exhibit decreased H3K27me3.** (A) Immunoblots of acid-extracted histones from DIPGs of different indicated H3 genotypes. (B) Immunoblots of histones from PDGF-induced gliomas with

and without the H3.3K27M transgene. (C) Immunohistochemistry of H3K27me3 in human or murine gliomas containing wild-type H3.3 or H3.3K27M. (D) Immunohistochemistry quantification of nuclei staining positive for H3K27me3 ( $P = 0.01$  for human DIPG, and  $P = 0.0001$  for murine gliomas with the unpaired  $t$  test).

tagged H3 exhibited a decrease in K36me2 (~2.7-fold) and K36me3 (~18.5-fold) on the G34R/V mutants, compared with wild type, as measured by mass spectrometry (fig. S2C). Heterotypic H3.3 G34R or G34V mononucleosomes were methylated to a lesser extent by recombinant SETD2 in vitro, which indicated that nonglycine residues at position 34 on the substrate peptide decreases SETD2 methylation at K36 (fig. S2, D and E).

H3K27me3 peptides allosterically stimulate PRC2 methyltransferase activity on nucleosome substrates (8, 9), and we found that incubation of 10 or 100  $\mu$ M of H3K27me3 peptide strongly stimulated PRC2 activity toward mononucleosome or oligonucleosome templates (Fig. 3A). Heterotypic H3K27M mono- or oligonucleosomes containing H3K27M (fig. S3, A and B) were methylated to a lesser extent than wild-type nucleosome substrates when purified human PRC2 was used (Fig. 3A and fig. S3C). This reduction in PRC2-dependent signal was unique to chromatin containing H3K27M, as heterotypic K27A, K27R, or K27Q mononucleosomes showed no decrease in methylation on the endogenous histone (Fig. 3B).

The reduced methylation on nucleosome templates suggested that the K27M peptide might interfere with PRC2 activity normally stimulated by H3K27me3. Incubation of K27M peptide in trans decreased PRC2 activity on wild-type nu-

cleosomes to below the no-peptide signal (Fig. 3C), whereas the unmodified or K27ac peptide exhibited little stimulation relative to no-peptide control (Fig. 3C). The H3K27M peptide reduced PRC2-dependent methylation by 6.2-fold at 45  $\mu$ M as measured by scintillation counting (Fig. 3D). Peptide titration showed that  $\mu$ M concentrations of H3K27M, but not the K27ac peptide, could inhibit PRC2-dependent methyltransferase activity in a dose-dependent manner (Fig. 3E and fig. S3, D and E).

We synthesized biotinylated H3 peptides carrying either the diazirine-containing methionine isostere L-photo-Met at position 27 (peptide 1) or a benzophenylalanine residue at position 31 that retains the K27M mutation (peptide 2) (fig. S4, F and G). Upon irradiation, both peptides cross-linked effectively to the EZH2 subunit and less so to the AEBP2 and EED subunits (Fig. 4A and fig. S4E), which suggested that K27M peptides inhibit PRC2 through interaction with the EZH2 active site. Although the EED subunit is needed for enzymatic activity and K27me3 allosteric activation (8), we did not observe interaction between EED and H3K27M peptides by surface plasmon resonance or peptide pull-down assays (fig. S4, A to D). We additionally found the K27M peptide could inhibit a PRC2 complex that contained a mutant EED (Y365A) that cannot interact with K27me3 (fig. S5A).

Titration of K27M peptide to in vitro methylation reactions revealed a median inhibitory concentration ( $IC_{50}$ ) of 5.9  $\mu$ M [95% confidence interval (CI) of 1.10 to 6.42]. To evaluate whether the thioether moiety of methionine was required for inhibition of PRC2, a norleucine derivative (K27Nle) was prepared. The K27Nle variant proved to be an even better inhibitor of PRC2 (Fig. 4B) ( $IC_{50}$  for K27Nle = 0.85  $\mu$ M) (95% CI: 0.57 to 1.27) (fig. S6A). Peptides containing Lys<sup>27</sup> replaced by Ile inhibited PRC2 to a lesser extent than K27M ( $IC_{50}$  for K27I = 8.9  $\mu$ M) (95% CI: 4.12 to 11.2), whereas Lys<sup>27</sup> replaced by Leu had no inhibitory effect on the amounts of H3K27me3 in vivo or PRC2 in vitro (Fig. 4C and fig. S6, B to D). Thus, a long, hydrophobic residue suffices for EZH2 binding, and methionine—and to a slightly lesser extent isoleucine—represents the ideal biochemically accessible choices.

SET domain histone methyltransferases contain several highly conserved aromatic residues that serve in substrate binding and catalysis. The Tyr<sup>641</sup> residue in EZH2 is hypothesized to restrict higher-order lysine methylation by acting as a steric gatekeeper (10, 11). Recombinant Y641N EZH2-containing PRC2 was less sensitive to inhibition by the H3K27M peptide compared with wild-type PRC2 (Fig. 4, D to F, and fig. S6, E and F), which furthers the argument that hydrophobic

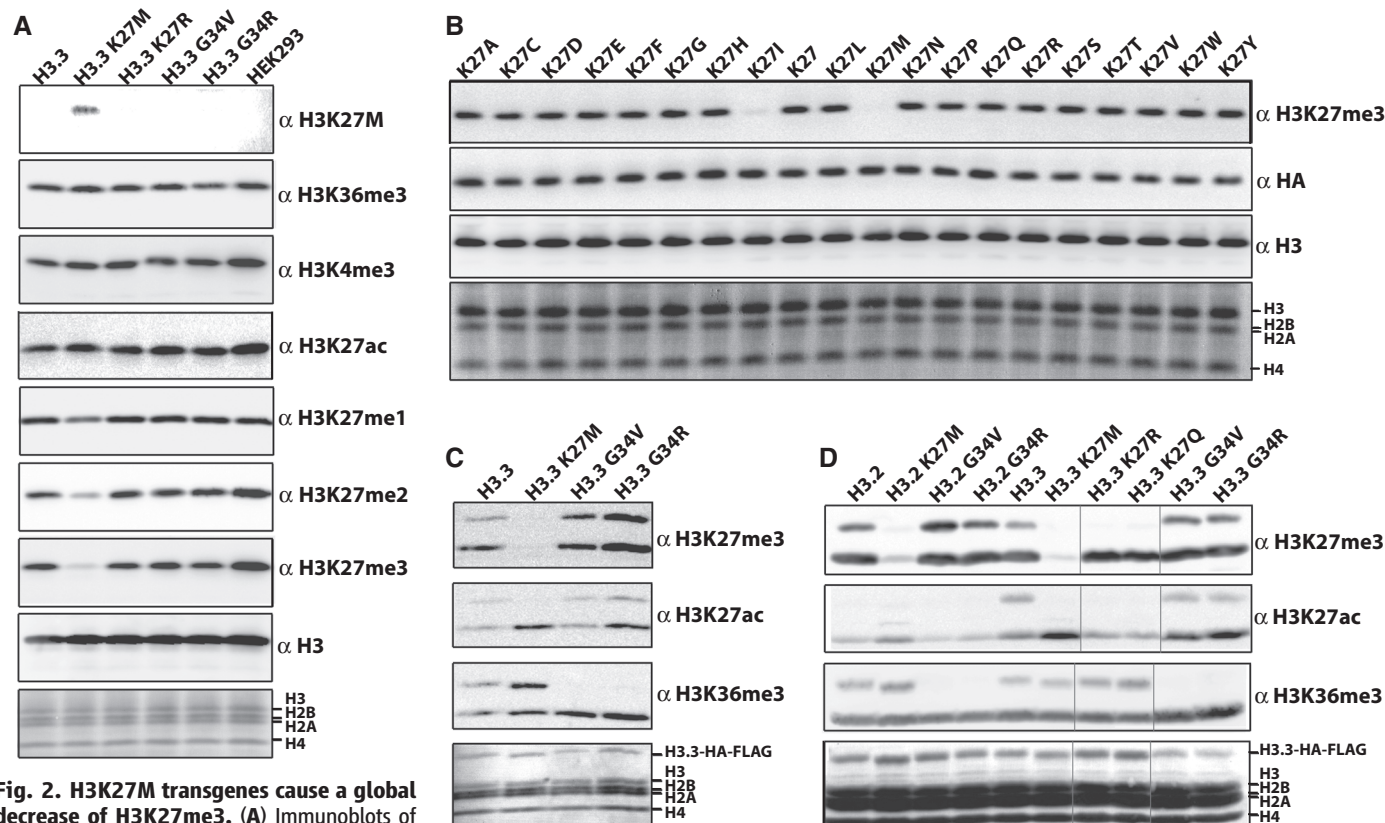


**Fig. 2. H3K27M transgenes cause a global decrease of H3K27me3.** (A) Immunoblots of whole-cell extract from lentivirus-transduced 293T cells expressing the indicated H3.3 transgenes. (B) Immunoblots of whole extract from H3.3 K27-to-X transduced 293T cells. The antibody against HA (anti-HA) blot shows the relative H3.3 transgene amounts. (C) Immunoblots of anti-HA-immunoprecipitated heterotypic H3.3 K27M or G34R/V mononucleosomes from

the indicated H3.3 transgenic 293T cell lines. (D) Immunoblots of anti-HA-immunoprecipitated oligonucleosomes (>95% of four to five nucleosomes in length, with a median of two to three nucleosomes) from the indicated H3.3 transgenic 293T cell lines (vertical black lines indicate where control lanes were removed for clarity).

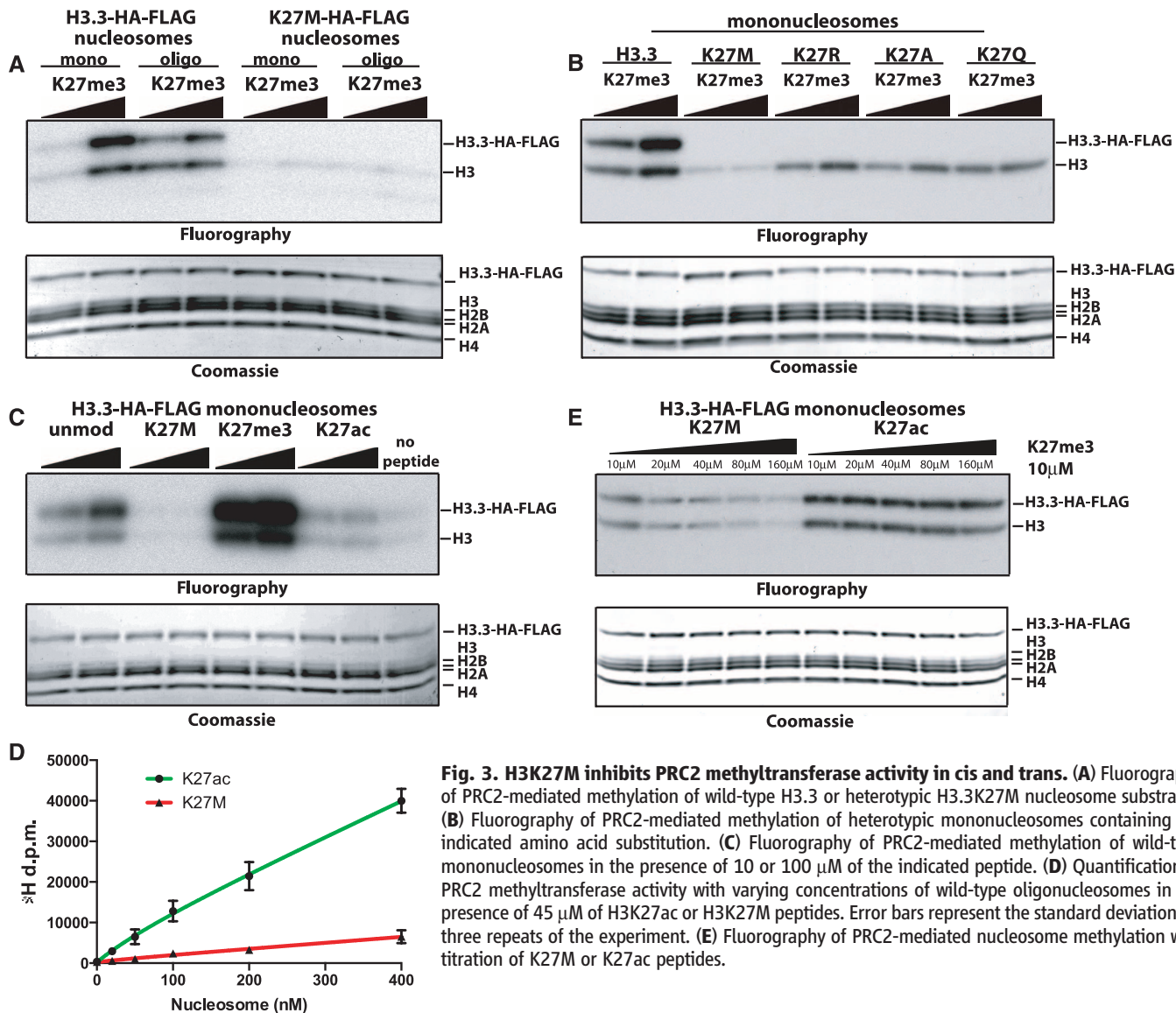


**Fig. 3. H3K27M inhibits PRC2 methyltransferase activity in cis and trans.** (A) Fluorography of PRC2-mediated methylation of wild-type H3.3 or heterotypic H3.3K27M nucleosome substrates. (B) Fluorography of PRC2-mediated methylation of heterotypic mononucleosomes containing the indicated amino acid substitution. (C) Fluorography of PRC2-mediated methylation of wild-type mononucleosomes in the presence of 10 or 100  $\mu$ M of the indicated peptide. (D) Quantification of PRC2 methyltransferase activity with varying concentrations of wild-type oligonucleosomes in the presence of 45  $\mu$ M of H3K27ac or H3K27M peptides. Error bars represent the standard deviation for three repeats of the experiment. (E) Fluorography of PRC2-mediated nucleosome methylation with titration of K27M or K27ac peptides.

interactions between the methionine side chain and aromatic residues in the EZH2 active site are important for K27M inhibition of PRC2.

We tested whether the highly conserved active sites of other SET-domain proteins may be similarly sensitive to methionine substitution at their cognate peptidyl-lysine substrate by constructing H3.3 transgenes containing methionine at K4, K9, and K36 (12). H3K9M and H3K36M transgenes decrease overall amounts of H3K9me2/3 and H3K36me2/3, respectively (Fig. 4G and fig. S7A). Although H3K4M transgenes did not diminish overall amounts of H3K4me2/3, the lack of reduction in methylation may be a consequence of reported inhibition of LSD1/2 histone H3K4me3 demethylases by H3K4M peptides (13). Histone H3K9M(1–20) peptides effectively inhibit recombinant histone H3K9 methyltransferases SUV39H1 and G9a (Fig. 4H) [ $IC_{50}$  for K9M = 2.2  $\mu$ M for SUV39H1 (95% CI: 1.7 to 2.6);  $IC_{50}$  for K9M = 3.6  $\mu$ M for G9a (95% CI: 2.1 to 5.9)] (fig. S7, B and C). These data argue that the H3K9-specific

SET-domain inhibition likely causes the reduction of H3K9me2/3 in H3.3K9M-expressing cells.

To determine whether the chromatin context of K-to-M mutants is important for in vivo inhibition of trimethylation, we placed the H3 tail (amino acids 1 to 42) onto the core domain (amino acids 23 to 102) of histone H4-HA-FLAG. H3K9me3 was reduced in cells expressing the K9M H3-H4 hybrid (fig. S8A). However, K27M and K36M failed to reduce H3K27me3 and H3K36me3 when expressed in the context of H3-H4 hybrid transgenes (fig. S8, B, C, and D). These results argue that SET-domain protein interactions with non-N-terminal nucleosomal surfaces are important for the full inhibitory activity of some K-to-M, but not all, mutants in vivo.

In summary, the data shown here provide compelling evidence that a missense histone mutation can dramatically alter nuclear biochemical processes through a gain-of-function mechanism. Moreover, our data indicate that K-to-M mutations target the active sites of diverse SET domain-

containing methyltransferases and, thereby, effectively compete with substrate binding and turnover. Notably, in their proper chromosomal context, K-to-M mutant histones that make up only a few percent of total histones suffice to prevent global methylation at their cognate residues. This reduction in histone methylation is expected to disrupt positive-feedback loops that contribute to the regulation of PRC2 and thus to enhance the inhibitory effect of mutant histones. We propose a model whereby aberrant epigenetic silencing through H3K27M-mediated inhibition of PRC2 activity promotes gliomagenesis. The broadly adaptable, yet highly specific, inhibition of SET-domain proteins through K-to-M mutation offers the intriguing possible existence of other etiological missense mutations in histones. Additionally, our work has uncovered a potentially useful mechanism to exclusively inhibit individual SET-domain methyltransferases, and conceivably other chromatin-modifying enzymes, implicated in a variety of malignancies.

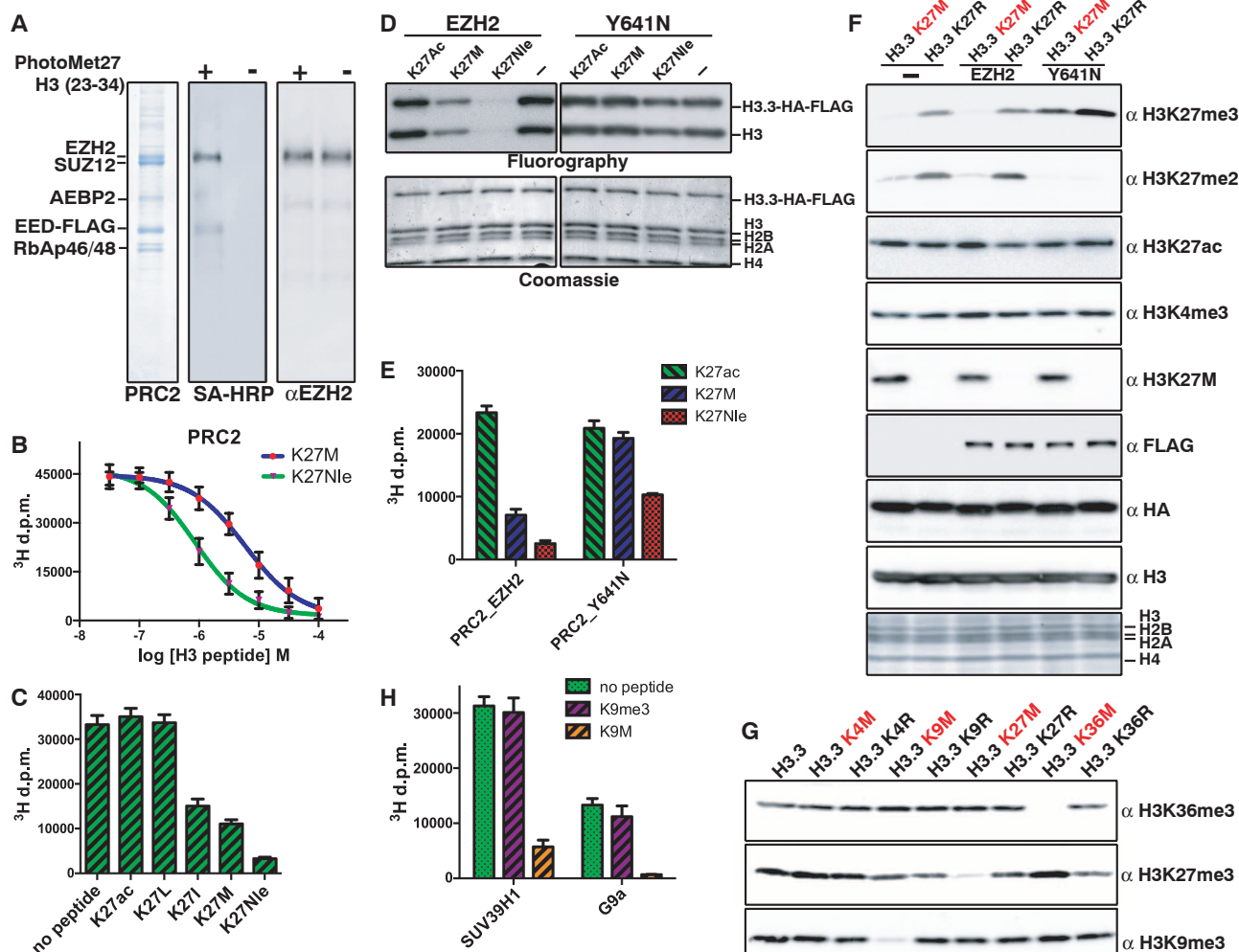


**Fig. 4. H3K27M-mediated inhibition of PRC2 occurs through interaction with EZH2.** (A) Coomassie gel of purified PRC2 cross-linked to peptide 1 (fig. S4F) and immunoblots with streptavidin–horseradish peroxidase (SA-HRP) or antibody against EZH2. (B)  $\text{IC}_{50}$  measurement for methionine or norleucine substitution at K27. Titration reactions of H3.3K27M or K3.3K27Nle peptides with 70 ng PRC2 and 0.8  $\mu\text{g}$  wild-type oligonucleosomes. Error bars represent the standard deviation of five repeats. (C) Quantification of PRC2 methyltransferase activity in the presence of 50  $\mu\text{M}$  of H3 peptides (18 to 37) containing K27acetyl, K27Leu, K27Ile, K27Met, or K27Nle. Error bars represent standard deviation of three repeats. (D) Fluorography of methyltransferase reactions with wild-type or EZH2-Y641N PRC2 on wild-type H3.3 nucleosomes in the presence of 50  $\mu\text{M}$  H3 peptides (18 to 37) with K27acetyl, K27Met, or K27Nle. Error bars represent the standard deviation of three repeats. (E) Quantification of methyltransferase activity of reactions in (D). Error bars represent the standard deviation of five repeats. (F) Immunoblots of 293T cells expressing the indicated EZH2 and H3.3 transgenes. The anti-HA blot shows relative H3.3 transgene amounts, and the anti-FLAG shows the relative EZH2 or Y641N amounts. (G) Immunoblots of whole-cell extract from transduced 293T cells expressing the indicated H3.3 transgenes. The arrows to the right of the total H3 blot point to the transgenic histone (red) or endogenous wild-type histone (black). (H) Quantification of histone methyltransferase activity on H3 peptides (1 to 20) by SUV39H1 or G9a in the presence of 10  $\mu\text{M}$  H3K9me3 or H3K9M or no peptide. Error bars represent the standard deviation for five repeats.

#### References and Notes

1. S. J. Elsässer, C. D. Allis, P. W. Lewis, *Science* **331**, 1145 (2011).
2. J. A. Simon, C. A. Lange, *Mutat. Res.* **647**, 21 (2008).
3. R. Margueron, D. Reinberg, *Nature* **469**, 343 (2011).
4. D. A. Khuong-Quang *et al.*, *Acta Neuropathol.* **124**, 439 (2012).
5. J. Schwartzentruber *et al.*, *Nature* **482**, 226 (2012).
6. G. Wu *et al.*, *Nat. Genet.* **44**, 251 (2012).
7. O. J. Becher *et al.*, *Cancer Res.* **70**, 2548 (2010).
8. R. Margueron *et al.*, *Nature* **461**, 762 (2009).
9. C. Xu *et al.*, *Proc. Natl. Acad. Sci. U.S.A.* **107**, 19266 (2010).
10. D. B. Yap *et al.*, *Blood* **117**, 2451 (2011).
11. C. J. Sneeringer *et al.*, *Proc. Natl. Acad. Sci. U.S.A.* **107**, 20980 (2010).
12. S. D. Taverna, H. Li, A. J. Ruthenburg, C. D. Allis, D. J. Patel, *Nat. Struct. Mol. Biol.* **14**, 1025 (2007).
13. A. Karytinos *et al.*, *J. Biol. Chem.* **284**, 17775 (2009).

**Acknowledgments:** B.A.G. acknowledges funding from NIH Innovator grant (DP2OD007447), Office of the Director, NIH. O.J. B. is supported by the U.S. Department of Defense; The Pediatric Brain Tumor Foundation; and the Damon Runyon, Rory David Deutsch, and Cristian Rivera Foundations. C.D.A. acknowledges funding from NIH (GM040922) and Starr Cancer Consortium

(grant SCC I6-A614). We thank D. Reinberg for reagents, and EMD Millipore for its role in H3K27M antibody generation.

#### Supplementary Materials

www.sciencemag.org/cgi/content/full/science.1232245/DC1  
Materials and Methods  
Supplementary Text  
Figs. S1 to S8  
Reference (14)

1 November 2012; accepted 12 March 2013  
Published online 28 March 2013;  
10.1126/science.1232245

RESEARCH

Open Access

# Pax3 expression enhances PDGF-B-induced brainstem gliomagenesis and characterizes a subset of brainstem glioma

Katherine L Misuraca<sup>1</sup>, Kelly L Barton<sup>2,3</sup>, Alexander Chung<sup>2,3</sup>, Alexander K Diaz<sup>4,5</sup>, Simon J Conway<sup>6</sup>, David L Corcoran<sup>7</sup>, Suzanne J Baker<sup>5</sup> and Oren J Becher<sup>2,3,8,9\*</sup>

## Abstract

High-grade Brainstem Glioma (BSG), also known as Diffuse Intrinsic Pontine Glioma (DIPG), is an incurable pediatric brain cancer. Increasing evidence supports the existence of regional differences in gliomagenesis such that BSG is considered a distinct disease from glioma of the cerebral cortex (CG). In an effort to elucidate unique characteristics of BSG, we conducted expression analysis of mouse PDGF-B-driven BSG and CG initiated in Nestin progenitor cells and identified a short list of expression changes specific to the brainstem gliomagenesis process, including abnormal upregulation of paired box 3 (*Pax3*). In the neonatal mouse brain, *Pax3* expression marks a subset of brainstem progenitor cells, while it is absent from the cerebral cortex, mirroring its regional expression in glioma. Ectopic expression of *Pax3* in normal brainstem progenitors *in vitro* shows that *Pax3* inhibits apoptosis. *Pax3*-induced inhibition of apoptosis is p53-dependent, however, and in the absence of p53, *Pax3* promotes proliferation of brainstem progenitors. *In vivo*, *Pax3* enhances PDGF-B-driven gliomagenesis by shortening tumor latency and increasing tumor penetrance and grade, in a region-specific manner, while loss of *Pax3* function extends survival of PDGF-B-driven;p53-deficient BSG-bearing mice by 33%. Importantly, *Pax3* is regionally expressed in human glioma as well, with high *PAX3* mRNA characterizing 40% of human BSG, revealing a subset of tumors that significantly associates with *PDGFRA* alterations, amplifications of cell cycle regulatory genes, and is exclusive of *ACVR1* mutations. Collectively, these data suggest that regional *Pax3* expression not only marks a novel subset of BSG but also contributes to PDGF-B-induced brainstem gliomagenesis.

**Keywords:** Brainstem Glioma, *Pax3*, DIPG, *ACVR1*

## Introduction

Brainstem Glioma (BSG) is a brain tumor that arises anywhere in the brainstem, and is seen predominately in children. Although BSG accounts for only 15-20% of all pediatric brain tumors, it is the leading cause of death for children with brain tumors [1]. The majority of BSG (80-85%) are high grade, diffuse, and are located in the pons—these are also known as Diffuse Intrinsic Pontine Glioma (DIPG) and have an overall survival of less than one year [1]. The term BSG hereafter will refer to high grade BSG or DIPG. Conventional focal radiation therapy

remains the standard-of-care for these tumors, with no documented additional benefit for any alternative treatment [2].

Genetic alterations commonly found in BSG include gains and/or activating mutations in platelet-derived growth factor receptor alpha (*PDGFRA*), amplification of genes involved in the receptor tyrosine kinase-Ras-phosphoinositide 3-kinase signaling pathway or cell cycle regulation, and a K27M mutation of histone H3.3 or 3.1 [3-9]. Recently, mutations in the *ACVR1* gene have been discovered in 20-32% of cases [10-13], as well as mutations in the *PPM1D* gene [11,14]. The most frequent tumor suppressor lost is *TP53*, with *INK4A-ARF* less commonly absent at the genomic level but possibly silenced through alternative mechanisms [3,6,15,16]. Previous work on BSG has characterized distinct subsets of the disease, including mesenchymal and oligodendroglial [5],

\* Correspondence: oren.becher@duke.edu

<sup>2</sup>Division of Pediatric Hematology-Oncology, Duke University Medical Center, Durham, NC, USA

<sup>3</sup>Preston Robert Tisch Brain Tumor Center, Duke University Medical Center, Durham, NC, USA

Full list of author information is available at the end of the article

N-Myc and Hedgehog [17], MYCN, silent, and H3-K27M [10] or H3-K27M and wildtype [6]. Together, these classifications highlight the heterogeneity of this disease and the likelihood that effective treatment will require an understanding of the mechanisms driving the growth of each individual subtype.

In addition to the heterogeneity within pediatric BSG, increasing evidence suggests that this disease is biologically distinct not only from adult glioma but also from pediatric supratentorial glioma in terms of genetic alterations and expression signatures [3-5]. Gliomas arising in the midline of the central nervous system (including the brainstem) commonly harbor the H3.3/3.1-K27M mutation only, while gliomas that arise in the cerebral cortex may contain an alternative H3.3-G34R/V mutation [6-9]. Regional differences in glioma may be a consequence in part of innate differences in the cells from which the tumors arise. Several studies have shown that NSCs from various regions of the brain differ in their capacity to respond to oncogenic stimuli *in vitro* and *in vivo* [18,19]. In addition, human infratentorial and supratentorial low-grade gliomas have distinct expression signatures corresponding to normal astrocytes and NSCs from their respective regions [20], while the expression patterns of G34R/V and K27M mutant gliomas mimic the developmental region in which they arise [8].

One gene found to be expressed at higher levels in infratentorial compared to supratentorial low-grade glioma is paired box 3 (*PAX3*) [20]. Pax3 is a developmental transcription factor that displays a regionalized expression pattern in the neural tube, neural crest, and somite of the vertebrate embryo, with expression decreasing as differentiation progresses [21]. Early in embryogenesis, Pax3 is transiently expressed in the posterior and dorsal neural tube [22-24]. This leads to its expression in the developing CNS to be localized to infratentorial structures such as the brainstem and cerebellum, but not to supratentorial domains such as the cerebral cortex (see P4 *in situ* hybridization for Pax3 in [25]). Pax3 is not only necessary for the proper specification of these developing tissues [21,26-28], but also for cell survival as homozygous loss of Pax3 in the mouse leads to severe neural crest and neural tube defects, attributable to an induction of p53-dependent apoptosis [29-31].

Ectopic expression of Pax3 is found to be pro-tumorigenic in sarcomas and neural crest-derived tumors such as melanoma and neuroblastoma [21]. However its role in glioma is less well-understood. Pax3 is re-expressed and upregulated in human glioma relative to normal brain tissue with its expression increasing concomitant with World Health Organization Grade and worsening prognosis, irrespective of tumor location [32]. Functionally, Pax3 has been implicated in promoting proliferation and invasion and inhibiting apoptosis

of glioma cell lines, and promoting growth of glioma subcutaneous xenografts [33].

In this study, we sought to gain insight into the unique attributes of BSG by comparing it to high-grade glioma of the cerebral cortex (CG). In an expression array comparing mouse BSG and CG induced by PDGF-B overexpression and Ink4a-ARF loss [34], we identified Pax3 as being a brainstem-specific marker. Pax3 is regionally expressed in the neonatal mouse brain as well, characterizing a subset of Nestin progenitors in the brainstem but not in the cerebral cortex. Ectopic overexpression of Pax3 in brainstem progenitors inhibits apoptosis *in vitro* and enhances PDGF-B-induced brainstem gliomagenesis *in vivo*, in a region-specific manner. In the absence of p53, while Pax3 no longer inhibits apoptosis, it increases proliferation *in vitro* and maintains its pro-tumorigenic role *in vivo*. Importantly, the regional expression pattern of Pax3 is mirrored in human glioma, revealing a subset of BSG with high *PAX3* expression that associates with alterations in *PDGFRA* and cell cycle regulatory genes and is exclusive of *ACVR1* mutations. These data suggest that regional expression of Pax3 contributes to PDGF-B-induced brainstem gliomagenesis and characterizes a subset of human BSG.

## Materials and methods

### Mice

Nestin-Tva (Ntv-a) and Ntv-a;Ink4a-ARF<sup>-/-</sup> [34] and Ntv-a;p53<sup>fl/fl</sup> mice [35] have been described. Olig2-eGFP-L10a [36,37] were bred to Ntv-a;Ink4a-ARF<sup>-/-</sup> mice to generate Ntv-a;Ink4a-ARF<sup>-/-</sup>;Olig2-eGFP-L10a mice. Pax3-floxed mice [38] were bred to Ntv-a;p53<sup>fl/fl</sup> mice to generate Ntv-a;p53<sup>fl/fl</sup>;Pax3<sup>fl/fl</sup> (Pax3-KO) and control Ntv-a;p53<sup>fl/fl</sup>;Pax3<sup>+/+</sup> mice. Nestin-CFPnuc mice have been previously described, and express the cyan fluorescent protein fused to a nuclear localization signal under the control of the regulatory elements of the Nestin gene [39]. For genotyping, gDNA was isolated from mice using the REDExtract-N-Amp Tissue PCR Kit (Sigma) per the manufacturer's protocol, using previously published primers. All work with mice was done in accordance with the Duke University Animal Care and Use Committee and the Guide for the Care and Use of Laboratory Animals.

### RCAS/Tv-a glioma mouse modeling

In the RCAS/Tv-a glioma mouse modeling system, avian retroviruses (produced from RCAS plasmids) infect mouse cells expressing Tv-a (the receptor for RCAS viruses). DF1 cells (ATCC) were cultured and transfected with RCAS plasmids as described [35] using Eugene 6 or X-TremeGENE 9 (Roche). RCAS-Y, RCAS-PDGF-B, and RCAS-Cre plasmids are described [40]. RCAS-Pax3 plasmid was obtained from Andrew Bendall (University of Guelph, Ontario) [41]. RCAS-H3.3-K27M

plasmid was generated by the C. D. Allis lab (The Rockefeller University, New York) [42]. Generation of PDGF-B-induced brainstem glioma [34,35] and cerebral cortex glioma [43] were as described. Briefly,  $1 \times 10^5$  DF1 cells transfected with RCAS plasmids and producing RCAS viruses, were injected into the brainstem or cerebral cortex of neonatal Ntv-a pups (postnatal day 2–4) in 1  $\mu$ L volume using a custom Hamilton syringe. Combinations of viruses were injected at a 1:1 or a 1:1:1 ratio, and RCAS-Y transfected DF1 cells were used as a negative control. Injected mice were monitored daily and euthanized with CO<sub>2</sub> upon appearance of signs of brain tumors (enlarged head, ataxia, weight loss up to 25%) or at 12 weeks post-injection in the absence of symptoms.

### FACS of Olig2-eGFP-L10a glioma

Brainstem or Cerebral Cortex Gliomas from Ntv-a; Ink4aARF<sup>-/-</sup>;Olig2-eGFP-L10a mice injected with RCAS-PDGF-B were harvested and dissociated into a single cell suspension as described [35]. Briefly, tissue was digested in papain (Worthington) and DNase (Sigma Aldrich) at 37°C, followed by three cycles of triturations in ovomucoid (Worthington) and centrifugation at 600 rpm. The resulting cells were passed through a 70  $\mu$ m strainer, an aliquot of cells was set aside for the unsorted control, and the remainder of cells were sorted using a FACSVantage sorter (BD Bioscience) by the Duke Cancer Institute Flow Cytometry Core into GFP+ and GFP- populations. Cell populations were centrifuged, washed in PBS, snap frozen and stored at -80°C for mRNA isolation.

### Immunofluorescence

Ntv-a or Nestin-CFPnuc pups were sacrificed at P3 and their whole brains were fixed in 4% PFA in PBS for 24 hours, cryopreserved in 30% sucrose in PBS for 24–48 hours, followed by embedding in OCT on dry ice/ethanol. Blocks were sectioned using either a Shandon or Leica Cryostat into 12  $\mu$ m thick sections in a sagittal orientation. Sections were rehydrated in PBS-T (0.1% Triton-X100) and blocked in PBS-T with 10% normal goat serum. Primary antibodies were diluted in PBS-T with 1% BSA overnight at 4 degrees, and secondary antibodies were diluted in PBS-T for 1 hour. Antibodies used were anti-PAX3 (DSHB, concentrated form, 1:200), and anti-GFP (Invitrogen, 1:200); AlexaFluor-488 and -594 secondary antibodies (Invitrogen) were used at 1:200. Slides were mounted with Vectashield with Dapi (Vector Laboratories) and imaged using a Zeiss Axio Imager.

In order to quantify PAX3 and Nestin expression, three Nestin-CFPnuc P3 mice were analyzed. High-powered (20x) pictures of the PAX3-expressing cells in each brainstem region (midbrain, dorsal pons, mid pons, and ventral pons) were taken, 1–3 images per region per section, until at least 6 sections were represented for each region. All

pictures were taken using a Zeiss Axio Imager and consistent camera settings. For the cerebral cortex, 2 random 20x images were taken in at least 6 sections per mouse. Using Metamorph Premier software, a threshold was set for positive Nestin and PAX3 staining in each image. For each marker, the same threshold was applied to each image across the dorsal, mid, and ventral pons regions for each section. For the midbrain region, the threshold for PAX3 was consistently lowered slightly to accommodate a lower intensity of the PAX3 staining compared to the other regions. The threshold for Nestin staining in the cerebral cortex was set separately, and remained the same for all sections and all mice. There was no positive nuclear PAX3 staining in any cerebral cortex section. The positive nuclei (size > 200) for each marker were then counted using Integrated Morphometry Analysis. A color threshold was then applied to each Nestin/PAX3 overlay (the same threshold was used across regions for each section), and the number of double-positive cells were counted as described above. The cell counts for each region per section were totaled, and the percentage of Nestin + cells that were double positive per region was calculated. The percentages were averaged together across sections of the same mouse to generate a mean percentage for each region per mouse.

### Mouse and human expression analysis

Frozen BSG and CG samples, along with brainstem and cerebral cortex from age-matched non tumor-bearing mice of the same genetic background (n = 3 for all groups), were sent to Expression Analysis (EA, Durham, NC) for total mRNA isolation and hybridization to Affymetrix GeneChip Mouse Genome 430 2.0 Arrays. Total mRNA samples isolated from Olig2-eGFP-L10a-positive PDGF-B;Ink4aARF<sup>-/-</sup> glioma cells were sent to EA for hybridization to the same arrays. Data was analyzed using Partek Genomics Suite (Partek Incorporated) for quality control, Robust Multi-Array (RMA) was used for normalization, and differentially expressed genes were determined by one-way ANOVA using the cutoffs described in the text.

Human BSG and CG samples with expression data available from St. Jude [4,44] were selected for analysis. Log-scale Robust Multiarray Analysis (RMA) from the *affy* [45] package in Bioconductor [46] was used for normalization to eliminate systematic differences across the arrays. Differentially expressed genes between brainstem and cerebral cortex glioma samples were identified using the *limma* [47] package in Bioconductor, which utilizes an empirical Bayes' approach for parameter estimation and significance testing. The False Discovery Rate (FDR) method was employed to control for multiple hypothesis testing. To compare gene expression differences within the brainstem samples, RMA normalization

was applied to the arrays where they were then classified based on their normalized PAX3 expression levels (probe 231666\_at). Arrays where PAX3 had a normalized expression value > 4 were classified as *PAX3-High*, while all others were classified as *PAX3-Low*. Identification of genes differentially expressed between the two groups was calculated using *limma* as described above. These same classifications of *PAX3-High* and *PAX3-Low* were used for associations with genetic alterations, where the genetic alterations were acquired from previously published data [4,9,11,48].

Human BSG and CG samples with expression data available from Necker-Sick Children [5] were selected for an independent analysis. The Agilent microarray data was processed and normalized using the *limma* [47] package in Bioconductor [46]. The normexp method (normal + exponential convolution model) was used to correct for background intensities. Quantile normalization was used to eliminate systematic differences across all of the arrays. Differentially expressed genes between brainstem and cerebral cortex glioma samples were determined using the methods described above for the first dataset. To compare gene expression differences within the brainstem samples, arrays were classified based on their PAX3 expression levels (probe name: A\_23\_P502706). Arrays with a PAX3 expression level > 7 were classified as *PAX3-High*, whereas all others were classified as *PAX3-Low*. Identification of genes differentially expressed between the two groups was calculated using *limma* as described above.

#### **In vitro infection of brainstem progenitors with RCAS viruses**

Normal brainstem was isolated from Ntv-a or Ntv-a;p53<sup>fl/fl</sup> postnatal day 3 (P3) pups and was digested and dissociated as described above for Olig2-eGFP-L10a tumors. Cells were cultured in DMEM supplemented with 10% FBS, 2 mM L-glutamine, 100 units/mL penicillin and 100 µg/mL streptomycin at 37°C and 5% CO<sub>2</sub>, and passaged a maximum of 3 times for experiments. Cells were plated in clear 6-well plates for Annexin V assays, clear 96-well plates for BrdU assays, and white-walled, clear-bottomed 96-well plates for Caspase 3/7 assays.

To concentrate RCAS viruses, DF1 cells transfected with RCAS plasmids were passaged a minimum of 6 times from transfection, and then passaged 1:12. After 3 days, virus-containing media was harvested, centrifuged to remove cell debris, filtered through 0.45 µm pores, and concentrated 100-fold using Retro-X Concentrator (Clontech) per the manufacturer's instructions.

Brainstem progenitors were plated and infected with RCAS viruses at 1:100. Assays were conducted 3–5 days post-infection, or were split when confluent and subsequently plated for assays. For BrdU assays, the Cell Proliferation ELISA, BrdU Colorimetric kit (Roche)

was utilized, per the manufacturer's instructions using a Molecular Devices Versa Max Tunable Microplate reader. Caspase 3/7 activity was measured using the ApoToxGlo Triplex assay (Promega) per the manufacturer's instructions using a Turner Biosystems Modulus Microplate Reader. To measure the percentage of cells staining positive for Annexin V, the FITC Annexin V Apoptosis Detection Kit I (BD Pharmingen) was utilized per the manufacturer's instructions. For cell counting experiments, 50,000 infected cells were plated in 6 well plates in duplicate. For each time point, 2 wells of each line were trypsinized and counted with a Sceptor 2.0 Cell Counter (Millipore). All experiments were done a minimum of three times on at least three independent preparations of progenitor cells.

#### **Tumor grading and immunohistochemistry**

Tumor samples fixed in 10% formalin were embedded in paraffin by the Duke Pathology Core and cut into 5 µm thick sections using a Leica RM2235 microtome. H&E staining was performed using standard protocols. Tumor grading was done using the following criteria: Grade II glioma indicated by increased cellular density only; Grade III glioma indicated by the presence of microvascular proliferation; Grade IV glioma indicated by the presence of pseudopalisading necrosis. Immunohistochemistry (IHC) was performed using an automated processor (Discovery XT, Ventana Medical Systems, Inc.). Anti-PCNA antibody (Calbiochem) was used at 1:2000.

#### **PCR**

DNA was isolated from frozen tumors using the DNeasy Blood and Tissue Kit (Qiagen) per the manufacturer's instructions. Detection of the recombined Pax3-floxed allele was performed using previously published primers [38] and 60°C annealing temperature. For RT-PCR (both conventional and real time), cultured cells or snap frozen tumors were processed for mRNA isolation using the RNeasy Mini kit (QIAGEN) per the manufacturer's protocol. cDNA was synthesized from total mRNA using SuperScript II and OligodT primer (Invitrogen). RT-PCR primers for PDGF-B, Forward: 5'-AGTGACCACTC-GATCCGCTCCT-3', Reverse: 5'- TTTGGGGCGTTTT GGCTCGCTG-3', 55°C annealing temperature. PDGF-B primers amplify both mouse and human PDGF-B cDNA. qRT-PCR reactions were set up with iQ SYBR Green Supermix (BioRad) and run on a Bio-Rad iQ5 Multicolor Real-Time PCR Detection System. Primers for *Pax3*, Forward: 5'- TCCATCCGACCTGGTGCCAT-3', Reverse: 5'- TTCTCCACGTCAGGCGTTG, and *Actin*, Forward: 5'- TATTGGCAACGAGCGGTTCC-3', Reverse: 5'- GGC ATAGAGGTCTTTACGGATGTC-3'; 60°C annealing temperature. Relative gene expression levels were generated

using the  $\Delta\Delta C_t$  method [49] using *Actin* as the reference gene.

### Western blot

Frozen tumors were either grinded with a mortar and pestle on liquid nitrogen followed by lysis in RIPA buffer containing 1x Protease Inhibitor Cocktail (Sigma Aldrich), 10 mM PMSF, 50 mM NaF, 1 mM  $\text{NaVO}_4$ , and 1 mM DTT or lysed and homogenized in the same buffer using a Glas-Col Variable Speed-Reversible Homogenizer set to a motor speed of 80 followed by sonication using a Branson Sonifier 250. Cleared and denatured lysates were run on a NuPAGE 4-12% Bis-Tris gradient gel (Invitrogen), and transferred onto nitrocellulose membrane using the iBlot (Invitrogen). Antibodies were diluted in Odyssey Blocking Buffer (Li-Cor) with 0.2% Tween-20. Blots were imaged using the Odyssey (Li-Cor) per the manufacturer's instructions. Antibodies used were: anti-PAX3 (DSHB, concentrated form, 1:1000) and anti-ACTIN (Santa Cruz Biotechnology, 1:500). Secondary antibodies from Li-Cor were used at 1:10,000 for IRDye800CW or 1:20,000 for IRDye680LT.

### Statistical analysis

Statistics were calculated using GraphPad Prism 5 software. *In vitro* assays were performed a minimum of 3 times using cells from at least 3 independent P3 litters. Data are represented as the mean with SEM, using student's paired t-test. qRT-PCR for *Pax3* in mouse tissue was analyzed using student's unpaired t-test. *In vivo* analyses were performed using log-rank test (for survival) and Fisher's exact test (for tumor penetrance and grade). For analyses of human data, unpaired t-test was used for the age at diagnosis of PAX3-Low versus PAX3-High tumors, and Fisher's exact test was used to test for significance of the association between high Pax3 expression and genetic alterations.

## Results

### Mouse Brainstem Glioma and Cerebral Cortex Glioma have distinct gene expression signatures

In order to identify regional differences in glioma, and in particular unique characteristics of those arising in the brainstem, we generated mouse Brainstem Glioma (BSG) and Cerebral Cortex Glioma (CG) by injecting RCAS-PDGF-B virus-producing cells into the brainstem or cerebral cortex, respectively, of postnatal day 2–4 (P2-4) Nestin-Tv-a(Ntv-a);Ink4aARF<sup>-/-</sup> mice (Figure 1a) [34,43]. The gene expression profiles of the resulting tumors were first compared to their normal tissue counterparts. Using an FDR-adjusted p-value <0.05 and fold-change  $\geq 2.0$ , 7,869 genes were differentially expressed between normal cortex (NC) and CG (Figure 1b, Additional file 1: Table S1), while 7,263 genes were altered in BSG compared to normal

brainstem (NBS) (Figure 1b, Additional file 2: Table S2). Of the latter group, 2,547 genes were specific to the brainstem gliomagenesis process and were not altered during gliomagenesis in the cerebral cortex (Figure 1b). In addition, the comparison between BSG and CG revealed only 23 genes differentially expressed between these two types of tumors (Figure 1b-c, Additional file 3: Table S3), including upregulation of *Irx5* and *Pax3* and downregulation of *Bmp4* and *Foxg1*. We were interested in genes that functionally contribute to the brainstem gliomagenesis process, and so when these 23 genes were intersected with the 2,547 BSG-associated genes, 10 probes, representing 8 brainstem-specific gliomagenesis genes, were identified (Figure 1b, Table 1).

The expression array comparing Brainstem and Cerebral Cortex Gliomas described above was conducted with whole tumor tissue. Therefore it is possible that non-neoplastic cells contributed to some of the expression differences. To investigate this, we utilized the Olig2-eGFP-L10a reporter strain [36,37], in which the eGFP-L10a fusion protein is expressed under the control of the Olig2 promoter. As Olig2 expression marks all tumor cells of our glioma model [34], this effectively labels tumor cells with GFP. Ntv-a;Ink4a-ARF<sup>-/-</sup>;Olig2-eGFP-L10a mice were injected with RCAS-PDGF-B into the brainstem or cerebral cortex to generate BSG or CG, respectively, within 4–6 weeks from injection (Additional file 4: Figure S1a). Tumors were harvested, dissociated, and sorted into GFP-positive and -negative populations. The GFP-positive fractions were analyzed for gene expression differences by microarray, and 118 genes were found differentially regulated between Olig2-BSG and Olig2-CG tumor cells (Additional file 4: Figure S1b, Additional file 5: Table S4). Importantly, of the 8 brainstem-specific gliomagenesis genes in Table 1, the genes highlighted in bold were also differentially regulated between Olig2-BSG and Olig2-CG cells, and presumably play a role in BSG tumor cell biology.

### Pax3 expression characterizes mouse Brainstem Glioma

Among the 8 brainstem-specific gliomagenesis genes identified in this screen, 3 independent probes for the developmental transcription factor paired box 3 (*Pax3*) showed upregulation in BSG over CG and over normal brainstem (Table 1, Figure 2a). This differential expression pattern was confirmed via qRT-PCR (Figure 2b). *Pax3* was undetectable by qRT-PCR in normal cerebral cortex or CG tissue (n = 3 for each, data not shown). Importantly, *Pax3* was also differentially expressed between Olig2-BSG and -CG cells, with increased expression in BSG relative to CG (Figure 2c, Additional file 5: Table S4). To determine whether *Pax3* expression is confined to the Olig2-tumor cell compartment of BSG, qRT-PCR for *Pax3* was conducted on the sorted GFP-positive

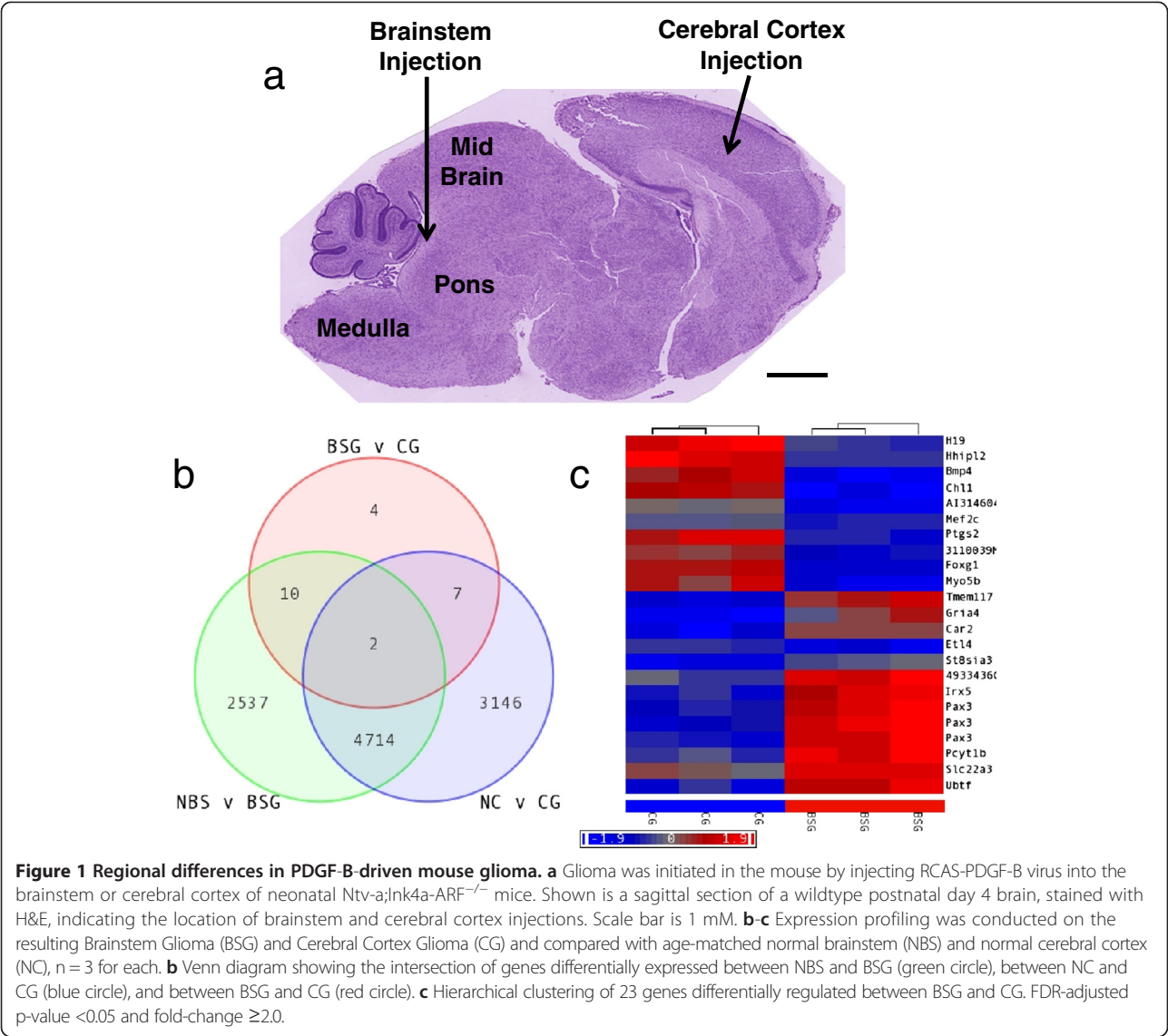


**Table 1 8 Genes associated with brainstem gliomagenesis but not cerebral cortex gliomagenesis and differentially expressed between Brainstem Glioma (BSG) and Cerebral Cortex Glioma (CG) in the mouse**

Gene symbol	Gene title	Fold-change BSG vs NBS	p-value	Fold-change BSG vs CG	p-value
<b>Pax3</b>	<b>paired box gene 3</b>	4.96	1.04E-05	8.44	1.20E-06
<b>Pax3</b>	<b>paired box gene 3</b>	3.87	2.19E-04	6.32	2.45E-05
<b>Irx5</b>	<b>Iroquois related homeobox 5 (Drosophila)</b>	3.35	2.67E-03	19.01	6.15E-06
<b>Pax3</b>	<b>paired box gene 3</b>	2.61	2.86E-04	3.70	3.24E-05
Pcyt1b	phosphate cytidyltransferase 1, choline, beta isoform	2.49	1.11E-05	2.46	1.24E-05
4933436C20Rik	RIKEN cDNA 4933436C20 gene	2.47	4.35E-05	2.99	1.08E-05
Myo5b	myosin VB	-2.41	5.53E-03	-7.59	2.41E-05
Bmp4	bone morphogenetic protein 4	-2.57	3.47E-07	-2.77	1.94E-07
<b>Chl1</b>	<b>cell adhesion molecule with homology to L1CAM</b>	-7.21	2.66E-06	-12.91	3.66E-07
Al314604	expressed sequence Al314604	-45.25	8.64E-11	-8.89	7.21E-09

Genes in bold are also differentially expressed between Olig2-eGFP-L10a BSG and CG (See Additional file 5: Table S4). NBS = Normal brainstem.

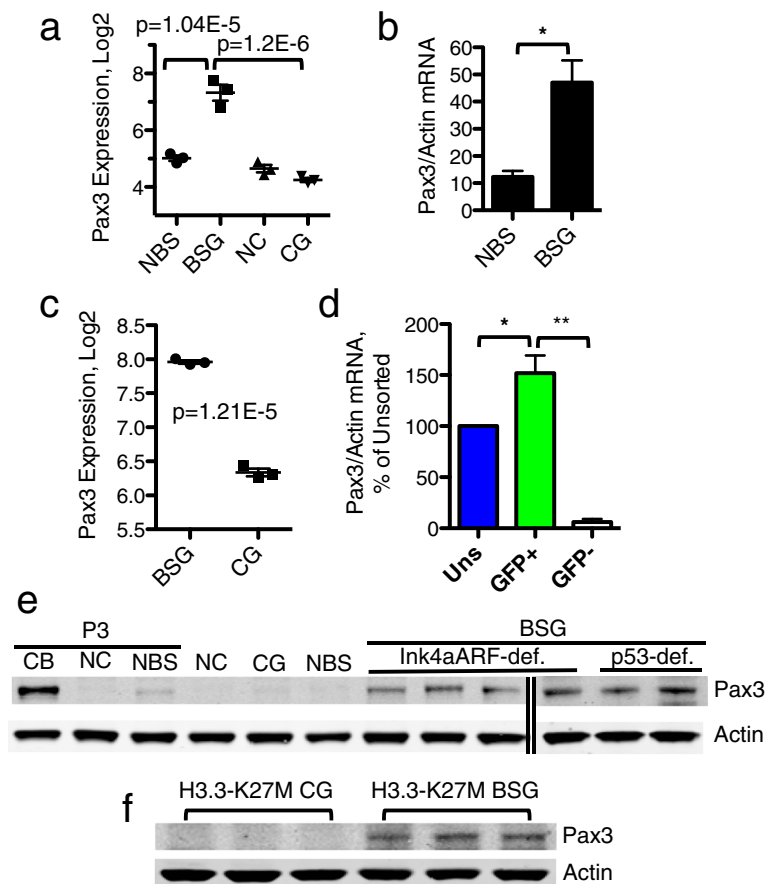


**Figure 2 Pax3 is expressed in mouse Brainstem Glioma.** **a** Log expression level of *Pax3* for one probe from the expression array in Figure 1. **b** qRT-PCR for *Pax3* in normal brainstem (NBS) and Brainstem Glioma (BSG) tissue,  $n = 3$  for each. Relative *Pax3* expression is normalized to *Actin*.  $p = 0.01$ , unpaired t-test. **c** Log expression level of *Pax3* for one of three probes from the Olig2-eGFP-L10a glioma expression array from Additional file 4: Figure S1b. **d** qRT-PCR for *Pax3* in unsorted (Uns), GFP+, and GFP- fractions of Olig2-eGFP-L10a BSG ( $n = 5$ ). *Pax3* expression levels are normalized to *Actin* and represented as a percentage of unsorted cells.  $p = 0.04$  Uns vs. GFP+,  $p = 0.002$  GFP+ vs. GFP-, paired t-test. **e** Western blot for PAX3 (53 kDa) in the following mouse tissues from left to right: P3 cerebellum (CB), P3 cerebral cortex (NC), and P3 brainstem (NBS); adult normal cerebral cortex (NC), Cerebral Cortex Glioma (CG), adult normal brainstem (NBS), and Brainstem Glioma (BSG). ACTIN (43 kDa) is shown as a loading control. **f** Western blot for PAX3 (53 kDa) in PDGF-B;H3.3-K27M;p53-deficient Cerebral Cortex Glioma (CG) and Brainstem Glioma (BSG). ACTIN (43 kDa) is shown as a loading control.

and -negative cells, relative to unsorted tumor cells. This revealed that *Pax3* expression is primarily found within the Olig2-tumor cell compartment of BSG (Figure 2d). *Pax3* mRNA was undetectable by qRT-PCR in all compartments of Olig2-eGFP-L10a CG ( $n = 3$ , data not shown).

PAX3 protein can also be detected at higher levels in mouse BSG than CG by western blot (Figure 2e). To determine whether high expression of PAX3 occurs in p53-deficient BSG, we injected Ntv-a;p53<sup>fl/fl</sup> mice with DF1 cells producing RCAS-PDGF-B and RCAS-Cre viruses [35]. In the tumors that arose in these mice, we found PAX3 protein expression at levels comparable to those found in Ink4aARF-deficient tumors (Figure 2e). In addition, to investigate whether the regional expression pattern of *Pax3* is relevant in the context of the

commonly occurring H3.3-K27M histone mutation, we injected Ntv-a;p53<sup>fl/fl</sup> mice with DF1 cells producing RCAS-PDGF-B, RCAS-H3.3-K27M, and RCAS-Cre viruses [42]. As shown in Figure 2f, we see high levels of PAX3 protein in PDGF-B;H3.3-K27M;p53-deficient gliomas initiated in the brainstem, but not in the cerebral cortex. Collectively, these data indicate that *Pax3* is a brainstem-specific marker of mouse PDGF-B-driven glioma in the context of Ink4aARF-deficiency, p53-deficiency, as well as H3.3-K27M expression.

#### Pax3 is regionally expressed in the neonatal mouse brain

High *Pax3* expression characterizes PDGF-B-driven mouse BSG while its expression is lower in glioma arising in the cerebral cortex. We speculated that enhanced PDGF signaling induced by PDGF-B ligand might upregulate *Pax3*

in the brainstem and be responsible for its high expression level. However, when brainstem progenitor cells isolated from Ntv-a P3 mice were infected *in vitro* with RCAS-PDGF-B virus, *Pax3* mRNA levels did not increase (Figure 3a).

As Pax3 is a developmental transcription factor whose expression normally decreases as differentiation proceeds, we next investigated whether Pax3 is expressed at the time of tumor initiation in the brainstem, which in our mouse model is P2-4. By Western blot, PAX3 protein was detected in wildtype P3 brainstem but not cerebral cortex (Figure 2e, cerebellum is shown as a positive control), consistent with its expression pattern in glioma. To further characterize the expression pattern of Pax3 in the developing brain, we conducted immunofluorescence for PAX3 protein in the P3 mouse brain and found several regions of expression within and around the developing brainstem. Distinct clusters of cells immunoreactive for PAX3 were found in the dorsal, mid, and ventral pons (Figure 3b-c, Additional file 6: Figure S2a-b, upper panels). In addition,

we found PAX3-positive cells lining the roof of the 4<sup>th</sup> ventricle and radiating up and out from there into portions of the midbrain, which lies just anterior to the mouse pons (Figure 3d-e, upper panels). PAX3-positive cells were also found occasionally lining the floor of the 4<sup>th</sup> ventricle (Additional file 6: Figure S2c, upper panels). By contrast, there were no PAX3-positive cells detected by immunofluorescence in the cerebral cortex (Figure 3f, upper panel).

We next investigated whether Pax3 expression characterizes any Nestin-progenitors, the targeted cell-of-origin in our glioma mouse model, in the P3 mouse brainstem. We conducted co-immunofluorescence for cyan fluorescent protein (CFP) and PAX3 in the P3 brain of Nestin-CFPnuc mice [39] which express CFP fused to a nuclear localization signal under the control of the Nestin promoter. PAX3 expression was found in a subset of Nestin progenitors in the dorsal pons, the roof and floor of the 4<sup>th</sup> ventricle, and the midbrain (Figures 3b, d, e, and Additional file 6: Figure S2c, lower panels, and quantified in Figure 3g). Conversely, we found very little to no

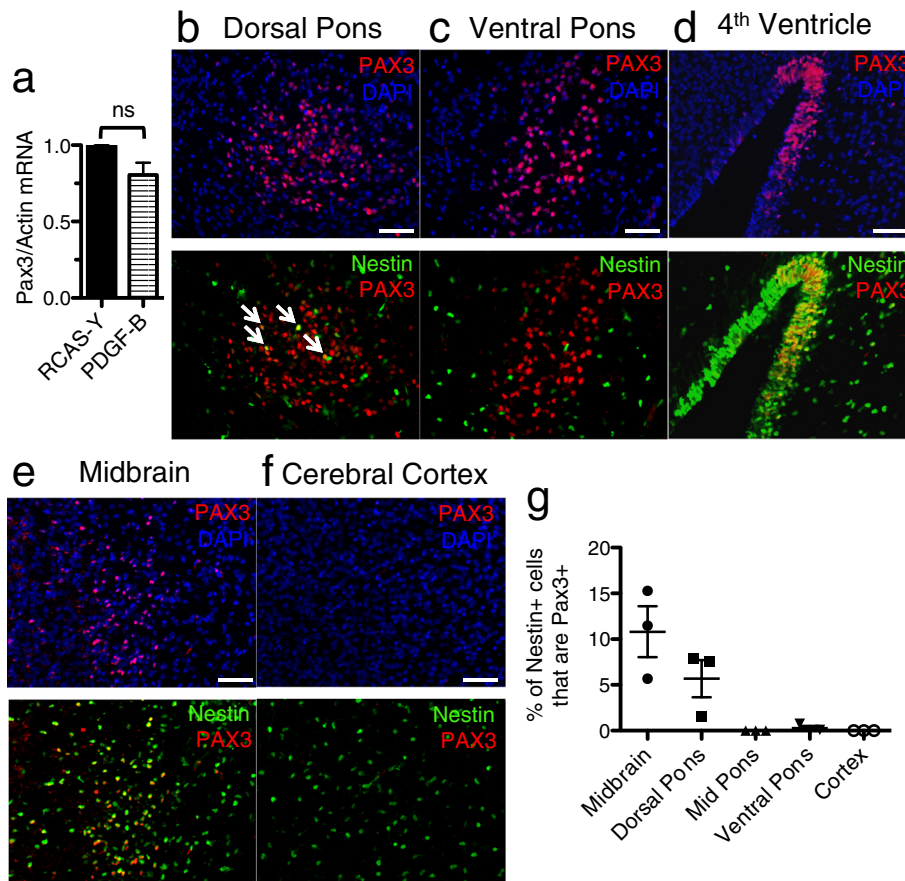


**Figure 3 Regional expression of Pax3 in the neonatal mouse brain.** **a** qRT-PCR for *Pax3* in RCAS-PDGF-B- versus RCAS-Y-infected brainstem progenitor cells. *Pax3* levels are normalized to *Actin*. **b-f** Immunofluorescence for PAX3 (red) and DAPI (blue) (upper panels), and PAX3 (red) and Nestin-CFP (green) (lower panels) in P3 Nestin-CFPnuc brain; 20x magnification, scale bar is 50  $\mu$ M in **b** dorsal pons (white arrows point to Nestin+/PAX3+ cells), **c** ventral pons, **d** 4<sup>th</sup> ventricle roof, **e** midbrain, **f** cerebral cortex. **g** The percentage of Nestin+ cells in each of the indicated brain regions that also express PAX3, quantified as described in the Methods section.

co-expression of Nestin and PAX3 in the ventral or mid pons and none in the cerebral cortex (Figure 3c, f, and Additional file 6: Figure S2b, lower panels, quantified in Figure 3g). Thus the regional expression pattern of Pax3, and its co-expression with Nestin, in the neonatal mouse brain correlates with its expression in glioma.

#### Pax3 inhibits apoptosis of brainstem progenitor cells

To investigate the functional role of Pax3 in brainstem progenitor cells, the brainstem region (including the midbrain and pons) from P3 Ntv-a mice was isolated, dissociated, and cultured *in vitro*. The Nestin-expressing progenitor cells were infected with RCAS-Y, RCAS-Pax3, RCAS-PDGF-B, or a 1:1 combination of RCAS-Pax3 and RCAS-PDGF-B (Figure 4a and Additional file 7: Figure S3a). RCAS-Pax3 alone, or in combination with PDGF-B, did not directly increase proliferation of brainstem progenitors based on BrdU incorporation (Additional file 7: Figure S3b). However, Pax3 inhibited basal apoptosis as evidenced by caspase 3/7 activation (Figure 4b). Similarly, Pax3 overexpression reduced the percentage of cells staining positive for Annexin V, a marker for early apoptosis, when compared to RCAS-Y-infected cells (Figure 4c).

#### Pax3 enhances PDGF-B-induced brainstem gliomagenesis *in vivo*

In order to determine if Pax3-induced inhibition of apoptosis is sufficient to induce glioma *in vivo*, P3 Ntv-a mice were injected in the brainstem with RCAS-Pax3, RCAS-PDGF-B, or a 1:1 mixture of both viruses. While PDGF-B overexpression alone led to asymptomatic low-grade glioma in 5 out of 20 mice, Pax3 overexpression alone did not lead to tumor formation (Figure 5a-c).

When compared to PDGF-B injection alone, the addition of Pax3 to PDGF-B significantly reduced survival (Figure 5a) and increased tumor penetrance to 20 out of 25 mice ( $p = 0.0003$ , Figure 5b). Importantly, addition of Pax3 to PDGF-B overexpression caused a subset of tumors to progress to high-grade glioma based on the presence of microvascular proliferation (0/5 PDGF-B versus 5/20 PDGF-B + Pax3 high-grade,  $p = 0.056$ , Figure 5b-c). The Pax3-induced high-grade gliomas harbored increased proliferation compared to the low-grade tumors induced by PDGF-B alone based on PCNA staining (Figure 5d). The pro-tumorigenic role of Pax3 in glioma is brainstem-specific, as co-injection into the cortex of both PDGF-B and Pax3 did not significantly reduce survival or increase tumor penetrance ( $p = 1.0$ ) or grade ( $p = 1.0$ ) compared to injection of PDGF-B alone (Additional file 8: Figure S4). Therefore, in the presence of enhanced PDGF-B signaling, Pax3 is sufficient to generate aggressive high-grade BSG, a feat that PDGF-B alone cannot achieve in the brainstem.

#### Pax3 promotes proliferation and gliomagenesis in the brainstem independent of p53

As the majority of human BSG are p53-deficient, we investigated the role of Pax3 in our BSG mouse model in the absence of this tumor suppressor. Brainstem progenitor cells were isolated from P3 Ntv-a;p53<sup>fl/fl</sup> mice and infected with RCAS-Cre to knock-out p53 along with either RCAS-Y or RCAS-Pax3. In the absence of p53, Pax3 overexpression no longer inhibited caspase 3/7 activation (Figure 6a). However, in these p53-deficient progenitor cells, Pax3 overexpression did lead to a significant increase

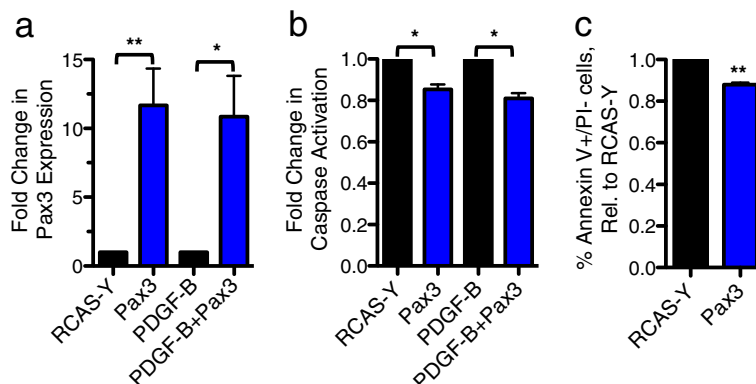


**Figure 4 Pax3 inhibits apoptosis of brainstem progenitor cells.** Brainstem progenitor cells from P3 Ntv-a mice were cultured *in vitro* and infected with the indicated RCAS viruses. **a** qRT-PCR for *Pax3* in the infected progenitor cells, normalized to *Actin*. Levels for Pax3-infected cells are expressed relative to RCAS-Y-infected cells,  $p = 0.007$  paired t-test, and levels for PDGF-B + Pax3-infected cells are expressed relative to PDGF-B-infected cells,  $p = 0.03$  paired t-test. **b** Caspase 3/7 activation of Pax3-infected cells is normalized to that of RCAS-Y-infected cells,  $p = 0.03$  paired t-test, while caspase 3/7 activation of PDGF-B + Pax3-infected cells is normalized to that of PDGF-B-infected cells,  $p = 0.02$  paired t-test. **c** Annexin V staining of RCAS-Pax3- versus RCAS-Y-infected progenitor cells. The percentage of Pax3-infected cells that were AnnexinV+/PI- was normalized to the percentage of RCAS-Y-infected cells that were AnnexinV+/PI-.  $p = 0.005$ , paired t-test.

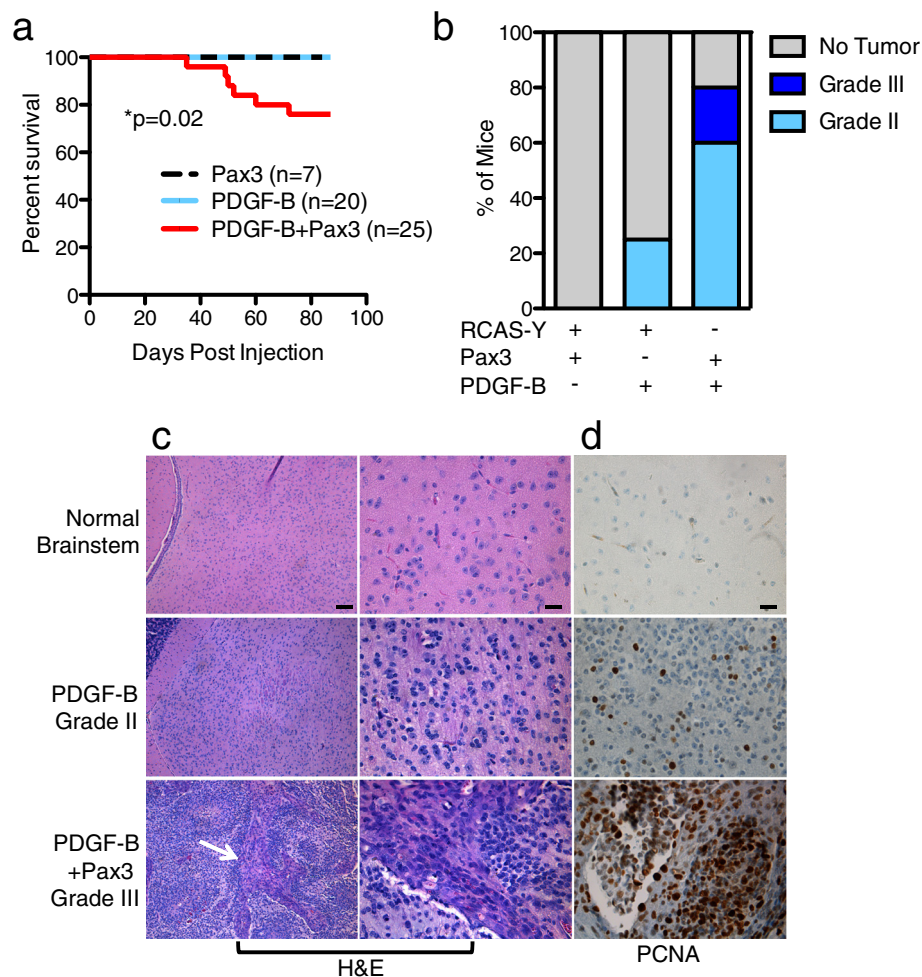


**Figure 5 Pax3 enhances PDGF-B-induced Brainstem Gliomagenesis.** **a** Kaplan-Meier survival curve of Ntv-a mice injected with DF1 cells expressing RCAS-Pax3, RCAS-PDGF-B, or RCAS-PDGF-B + RCAS-Pax3. **b** Mice from **(a)** were sacrificed at the onset of tumor symptoms or at 12 weeks in the absence of symptoms. Brains were harvested, fixed in formalin, and analyzed for the presence of tumors using hematoxylin and eosin (H&E) staining, and the tumors graded as described in Materials and Methods. Shown is the percentage of mice in each group with no tumor, grade II glioma, and grade III glioma. **c-d** Representative H&E staining **(c)** and IHC for proliferating cell nuclear antigen, PCNA **(d)** of normal brainstem (top row), PDGF-B-induced grade II BSG (middle row), and PDGF-B + Pax3-induced grade III BSG (bottom row). **c** Magnification is 10x in the left panels and 40x in the right panels. White arrow in lower-left panel indicates microvascular proliferation, which is enlarged in the 40x panel to its right. Scale bar for 10x is 100  $\mu$ M, 40x is 25  $\mu$ M. **d** 40x magnification; Scale bar is 25  $\mu$ M.

in cell proliferation, indicated by BrdU incorporation (Figure 6b) and cell counting (Figure 6c-d).

In order to test whether Pax3 is functionally required for the initiation or progression of p53-deficient BSG *in vivo*, we crossed conditional Pax3 knockout mice [38] into our p53-deficient BSG model [35]. Neonatal Ntv-a;p53<sup>fl/fl</sup>;Pax3<sup>fl/fl</sup> mice (Pax3-KO) and Ntv-a;p53<sup>fl/fl</sup>;Pax3<sup>+/+</sup> mice (Control), were injected with RCAS-PDGF-B and RCAS-Cre. Although both groups of mice succumbed to high-grade BSG, the Pax3-KO mice displayed a significant 33% increase in survival (median survival 38 days versus 28.5 days, Figure 6e). Recombination of the Pax3-floxed allele was confirmed via PCR of gDNA and loss of PAX3 protein expression was confirmed via

Western blot in Pax3-KO tumors (Additional file 9: Figure S5a-b). The increased survival of Pax3-KO mice suggests that Pax3 functionally contributes to brainstem gliomagenesis, although it is ultimately not required as tumors can quickly evade the loss of Pax3.

#### High Pax3 expression defines a novel subset of human BSG

To correlate our observations regarding Pax3 expression and function in mouse glioma with human disease, pediatric BSG (all of which were characterized as DIPG) and CG samples were utilized from previously published gene expression profiles, one comprised of post-treatment autopsies [4,44], and one comprised of pre-treatment

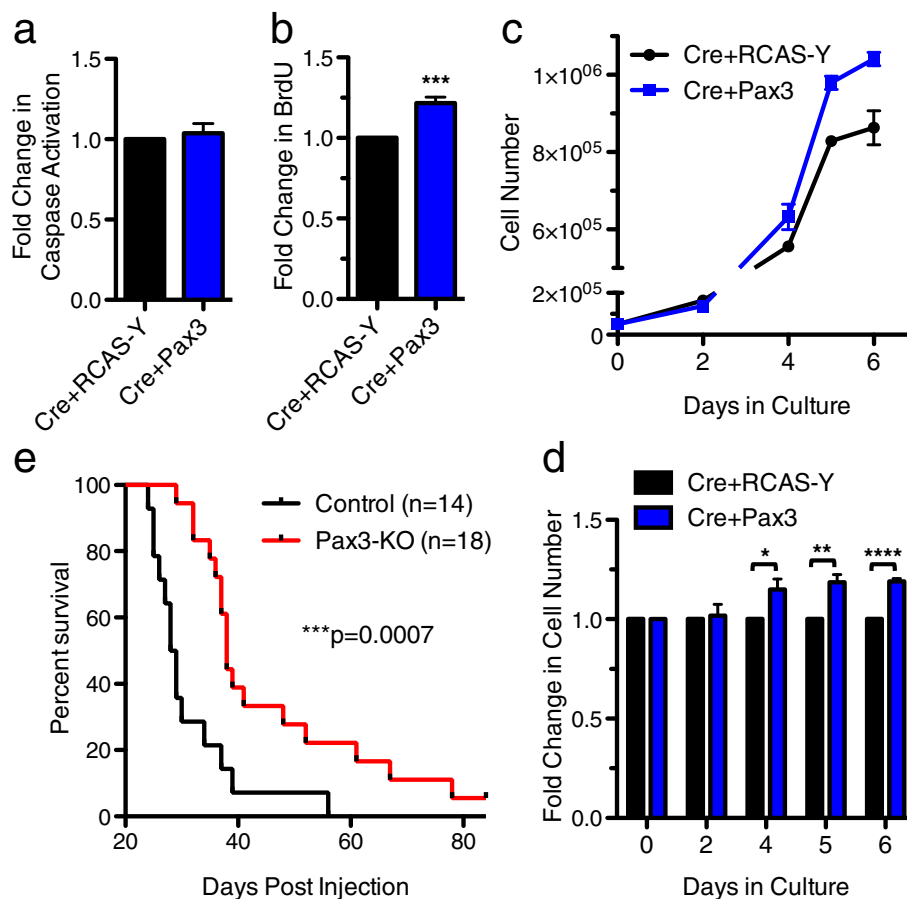
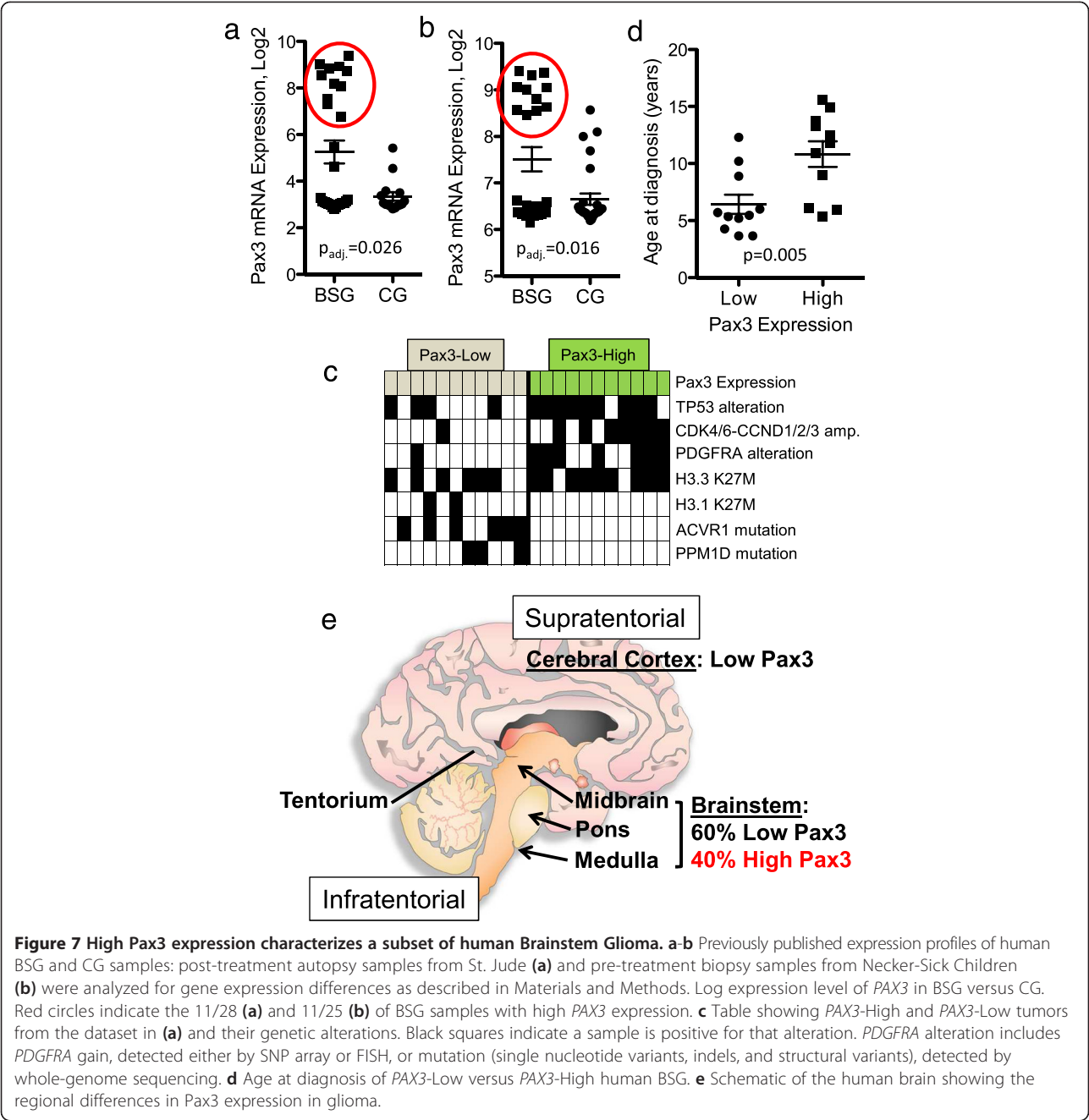


**Figure 6 Pax3 promotes proliferation *in vitro* and brainstem gliomagenesis *in vivo* in the absence of p53.** **a-d** Brainstem progenitor cells from P3 Ntv-a;p53<sup>fl/fl</sup> mice were cultured *in vitro*, infected with the indicated RCAS viruses, and assayed for **(a)** Caspase 3/7 activity at 72 hours after plating, normalized to Cre + RCAS-Y, **(b)** BrdU incorporation at 72 hours after plating, normalized to Cre + RCAS-Y,  $p = 0.0007$  paired t-test, and **(c-d)** cell number at the indicated time points after plating. **c** One representative experiment conducted in one progenitor line. **d** The fold change in Cre + Pax3 cells over Cre + RCAS-Y cells at each time point compiled from multiple progenitor lines,  $p = 0.03$  (day 4),  $p = 0.005$  (day 5),  $p < 0.0001$  (day 6), paired t-test. **e** Kaplan-Meier survival curve of Ntv-a;p53<sup>fl/fl</sup> mice (Control) and Ntv-a;p53<sup>fl/fl</sup>;Pax3<sup>fl/fl</sup> mice (Pax3-KO) injected with RCAS-PDGF-B + RCAS-Cre into the brainstem at P2-4.

biopsies [5]. The BSG and CG profiles from each dataset were compared, generating lists of significantly differentially expressed genes (FDR-adjusted  $p$ -value  $< 0.05$ , Additional file 10: Table S5 and Additional file 11: Table S6). *PAX3* was upregulated in BSG relative to CG in both datasets, 3.7-fold in the autopsy samples (Figure 7a), and 1.8-fold in the biopsy samples (Figure 7b).

Interestingly, high *PAX3* expression characterized approximately 40% of the BSG samples in both datasets (11/28, Figure 7a, and 11/25, Figure 7b). To glean information regarding the tumors with high *PAX3* expression, we first compared gene expression profiles of the *PAX3*-Low versus *PAX3*-High BSG samples from both datasets. Besides *PAX3*, there were very few genes that met the criteria for significance (adjusted  $p$ -value  $< 0.05$ , Additional file 12: Table S7 and Additional file 13: Table S8), and none that shed any additional light on the biology of the *PAX3*-High subset. We next compared

the genetic alterations occurring in *PAX3*-Low versus *PAX3*-High BSG samples from Figure 7a [4,9,11,48]. As is shown in Figure 7c, Table 2, and Additional file 14: Table S9, high *PAX3* expression significantly associated with wildtype *ACVR1*, *PDGFRA* amplification or mutation, and *CDK4/6-CCND1/2/3* amplification. In addition, *PPM1D* and H3.1-K27M mutations were found exclusively in *PAX3*-Low tumors (27% and 18%, respectively), although these relationships were not significant due to their low frequency. The majority of *PAX3*-High tumors also contained *TP53* alterations (82%) and the H3.3-K27M mutation (82%). Lastly, compared to children with *PAX3*-Low BSG, those harboring *PAX3*-High BSG were significantly older at diagnosis (Figure 7d). Collectively, these data describe a novel subset of human BSG with high Pax3 expression that are commonly characterized by increased PDGF signaling, and highlight an important regional difference between



pediatric gliomas arising in the cerebral cortex (supratentorial) and the brainstem (infratentorial) (Figure 7e).

**Discussion**

Brainstem Glioma (BSG) is a distinct disease, biologically and clinically, from glioma of the cerebral cortex (CG). While decades of research has provided insight into the cellular, molecular, and genetic alterations occurring in CG and guided therapeutic strategies for that disease, the field of BSG research is still in its infancy. In an effort to identify unique characteristics of BSG, we compared gene expression profiles of mouse PDGF-B-induced BSG and CG, and identified 23 genes that are differentially regulated between gliomas arising in the two regions. Among those genes, 8 were associated with the gliomagenesis process in the brainstem but not in the cerebral cortex—these genes we identify as “brainstem-specific gliomagenesis genes”. Of these genes, *Pax3*, *Irx5*, and *Chl1* were also differentially regulated between the Olig2-compartments of BSG and CG suggesting that they represent biological differences within the tumor cells. As Olig2 characterizes the majority of human BSG, particularly the oligodendroglial (PDGFRA)

**Table 2 Genetic alterations associated with Pax3 expression in human Brainstem Glioma**

Genetic alteration	Pax3-low	Pax3-high	P-value <sup>b</sup>
ACVR1 mutation	6/11	0/11	*0.01
PDGFRA alteration <sup>a</sup>	1/11	7/11	*0.02
CDK4/6-CCND1/2/3 amp	1/11	7/11	*0.02
TP53 alteration	4/11	9/11	0.08
PPM1D mutation	3/11	0/11	0.2
Histone H3.3-K27M	6/11	9/11	0.4
Histone H3.1-K27M	2/11	0/11	0.5

<sup>a</sup>Includes PDGFRA gain, detected either by SNP array or FISH, or mutation (single nucleotide variants, indels, and structural variants), detected by whole-genome sequencing.

<sup>b</sup>Fisher's Exact Test.

\*p-value < 0.05.

and H3-K27M subgroups [5,8,50,51], as well as marks a candidate cell-of-origin for BSG [52], the expression profile of these cells has important implications for at least a subset of the human disease.

Due to the controlled nature of this experiment, the gene expression signatures identified in this study can be primarily attributed to regional characteristics of the brainstem and cerebral cortex. It has not been previously reported that gliomas induced with the same genetic alterations in different regions of the mouse brain have distinct gene expression. We have found mouse BSG to harbor a distinct expression pattern of developmental homeobox genes and transcription factors, including *Pax3*, *Irx5*, *Foxg1*, and *Lhx2*. Overall, these observations are similar to those made by others in comparing human infratentorial to supratentorial low-grade glioma [20], and BSG to other pediatric high-grade glioma [5]. The latter study did not include *PAX3* in their list of genes upregulated in BSG, however, potentially due to the inclusion of thalamic gliomas in their high-grade glioma group, some of which could harbor high *PAX3* expression.

Herein is the first report of Pax3 expression in BSG. Importantly, we find regional expression of Pax3 in mouse PDGF-B-driven glioma in the context of Ink4aARF-loss, p53-loss, and overexpression of H3.3-K27M that is mirrored in human glioma. *PAX3* mRNA is expressed at higher levels in BSG compared to CG in two independent sets of human samples, which include both pre-treatment biopsies and post-treatment autopsies. The analyses also revealed that approximately 40% of human BSG harbor relatively high *PAX3* expression and that these tumors associate with increased PDGFRA signaling and alterations of cell-cycle regulatory genes, both of which characterize our PDGF-B-driven BSG mouse model. The majority of *PAX3*-High tumors also contain *TP53* alterations and the H3.3-K27M mutation, genetic alterations that also coexist with Pax3 expression in our mouse model. Collectively, these data suggest that *PAX3*-High tumors may be part of

the oligodendroglial and the H3-K27M subgroups previously described to harbor *PDGFRA* alterations [5,10]. In addition, *PPM1D*, H3.1-K27M, and *ACVR1* mutations occur only in *PAX3*-Low tumors. *ACVR1* mutations have also been reported to be mutually exclusive of *PDGFRA* alterations [11,13], although as we did not observe a link between PDGF signaling and *PAX3* expression, we believe the exclusivity between high *PAX3* and *ACVR1* mutation to be independent of *PDGFRA*. Consistent with *ACVR1* mutations occurring in younger patients [11], Pax3-High (and thus *ACVR1* wildtype) tumors are associated with older patients in this study.

The regional expression pattern of Pax3 in glioma correlates with its expression in the developing mouse brain, pointing to the possibility that the expression level of Pax3 in different regions of the developing brain dictate its expression level in gliomas arising in those regions. It is plausible that Pax3 is highly expressed in BSG because the gliomagenesis process prevents its normal downregulation, although this has not been directly tested. In support of this, however, several populations of Pax3-positive progenitor cells exist throughout the P3 mouse brainstem. A subset of these cells co-express the stem/progenitor cell marker Nestin, particularly in the dorsal pons and midbrain, locations in the mouse in which Pax3-High BSG are localized. As Nestin cells are the targeted cell-of-origin for the BSG model used here, it is possible that Nestin+/Pax3+ progenitors give rise to Pax3-High glioma in this mouse model. Although a Nestin+ cell is a candidate cell-of-origin for human glioma [53], the cell type(s) and the location of the cell(s) giving rise to human BSG specifically are still in question. The majority of human BSG are at diagnosis localized primarily to the ventral pons, suggesting a potential ventral location for the cell-of-origin [52]. This would be in contradiction to a dorsal Nestin+/Pax3+ cell-of-origin as discussed here, and represents a limitation of this model. However we do not yet know the identity or location of any Nestin+/Pax3+ progenitors in the developing human pons, and as there are significant differences between mouse and human brainstem anatomy, we cannot be certain that the dorsal Nestin+/Pax3+ progenitors identified here in the mouse correlate with a dorsal location in the human pons. Further investigation into the expression of Pax3 along with other glioma markers in the developing mouse and human brainstem will be the focus of future studies to hopefully clarify this issue.

Investigation into the function of Pax3 in the brainstem revealed that ectopically expressed Pax3 is not oncogenic in the absence of any other genetic alterations. While *in vitro*, Pax3 overexpression inhibits basal apoptosis, this effect is insufficient to induce tumor formation *in vivo*. When combined with the pro-proliferative effects of increased PDGF signaling, a common event found in *PAX3*-High human BSG, ectopic Pax3 enhances gliomagenesis,

increasing tumor frequency and promoting progression to a high-grade malignancy. Although we are unable to determine the percentage of tumor cells expressing both ectopic PDGF-B and Pax3 in this model, the survival advantage associated with both seen here suggests that the tumorigenesis process would select for doubly infected cells.

Pax3-induced inhibition of apoptosis is seemingly dependent on p53, as deletion of p53 in brainstem progenitors *in vitro* abolishes the anti-apoptotic effects of Pax3. This is in accordance with literature describing a direct interaction between Pax3 and p53 proteins leading to degradation of p53 [30,54]. Interestingly, in the absence of p53, Pax3 promotes the proliferation of brainstem progenitors, which may explain how deletion of Pax3 in p53-deficient BSG delays gliomagenesis *in vivo*. These pro-survival effects of Pax3 suggest that it can cooperate with other oncogenic drivers, either through inhibition of p53-dependent apoptosis or by promoting proliferation, functions that it provides to other types of cancer cells, including glioblastoma cell lines [33,55-57]. It should be noted that the *in vitro* experiments described here were conducted in the presence of serum, which induces differentiation. As Pax3 function is most likely dependent upon differentiation status, studying the effects of Pax3 in the context of stem cell conditions should be a focus of future research.

Collectively, our functional data suggest that Pax3 is able to promote the initiation as well as the progression of brainstem gliomagenesis when combined with other genetic alterations. As Pax3 has been found expressed in cerebral cortex glioma [32], infratentorial low-grade glioma [20], as well as high grade BSG as shown here, it appears that Pax3 is expressed in glioma (albeit at different levels) regardless of the tumor grade or location, and may play a functional role in all scenarios dependent on the context of additional genetic alterations. We find here that Pax3 increases the frequency of both low- and high-grade BSG in the context of PDGF signaling, supporting its role as an oncogene in both low- and high-grade brainstem lesions. Although results herein show a lack of Pax3 upregulation and function in cerebral cortex gliomas of mice, Chen et al. showed that Pax3 levels correlate with increasing WHO grade of supratentorial gliomas [32] and subsequently Xia et al. showed that Pax3 functionally promotes survival of GBM cell lines and xenografts originally isolated from supratentorial tumors [33]. Based on our direct comparison between BSG and CG, we would expect the levels of Pax3 expression in these supratentorial gliomas to be lower than in BSG. The functional discrepancies could be explained by varying contexts of genetic alterations, differences between mouse and human tumor biology, or an inhibitory effect on Pax3 expression or function of the cerebral cortex stroma in mice.

In summary, the data presented here show that mouse BSG and a subset of human BSG highly express Pax3, distinguishing these tumors from gliomas arising in the cerebral cortex. This expression pattern of Pax3 is mirrored in the developing brain, which may account for the gene's regional specificity in glioma. We have identified a subset of human BSG with high *PAX3* expression that associates with *PDGFRA* alterations and amplification of cell-cycle regulatory genes, and is exclusive of *ACVR1* mutations. Functional studies show that in addition to being a regional marker for BSG, Pax3 also inhibits apoptosis and promotes proliferation of brainstem progenitor cells, and contributes to PDGF-B-induced brainstem gliomagenesis *in vivo*. Important complements to these studies in the future will be to investigate the function of Pax3 in human BSG cells, both in cell lines and xenografts, as well as in epigenetically-induced models to study how the presence of the H3.3-K27M mutation contributes to or alters Pax3 function. Further investigation into the mechanisms upstream and downstream of Pax3 will increase our understanding of this subset of BSG and may lead to the identification of targets or pathways that could be exploited for therapeutic purposes.

## Additional files

**Additional file 1: Table S1.** Differentially expressed genes between mouse normal cortex (NC) and Cerebral Cortex Glioma (CG), FDR-adjusted p-value < 0.05, fold-change  $\geq 2$ .

**Additional file 2: Table S2.** Differentially expressed genes between mouse normal brainstem (NBS) and Brainstem Glioma (BSG), FDR-adjusted p-value < 0.05, fold-change  $\geq 2$ .

**Additional file 3: Table S3.** Differentially expressed genes between mouse Brainstem Glioma (BSG) and Cerebral Cortex Glioma (CG), FDR-adjusted p-value < 0.05, fold-change  $\geq 2$ .

**Additional file 4: Figure S1.** Regional differences in Olig2-Glioma cell compartments. a Kaplan-Meier survival curve of *Ntv-a;lnk4a-ARF<sup>-/-</sup>;Olig2-eGFP-L10a* mice injected with RCAS-PDGF-B into the brainstem or cerebral cortex at P2-4 to generate Brainstem Glioma (BSG) and Cerebral Cortex Glioma (CG), respectively. b Gliomas from (a) were harvested, dissociated, and sorted into GFP+ and GFP- compartments by FACS and the GFP+ BSG and CG samples (n = 3 for each) were compared using expression profiling. Shown is hierarchical clustering of 118 genes differentially regulated between BSG and CG Olig2-cells. p < 0.01 and fold change  $\geq 2.0$ .

**Additional file 5: Table S4.** Differentially expressed genes between Olig2-eGFP-L10a gliomas initiated in the brainstem (BS) and the cerebral cortex (CX), p-value < 0.01 and fold change  $\geq 2.0$ .

**Additional file 6: Figure S2.** Regional expression of Pax3 in the neonatal mouse brain. a Immunofluorescence for PAX3 (red) in P3 *Ntv-a* pons. Nuclei are stained with DAPI (blue). 10x magnification, scale bar is 100  $\mu$ M. White boxes indicate dorsal, mid, and ventral pons populations of PAX3-expressing cells. 4<sup>th</sup> ventricle and Cerebellum (Cb) are indicated for reference. b-c Immunofluorescence for PAX3 (red) and DAPI (blue), upper panels; PAX3 (red) and Nestin-CFP (green), lower panels. 20x magnification, scale bar is 50  $\mu$ M. b mid pons, c 4<sup>th</sup> ventricle floor: left panels are representative of the majority of sections analyzed in which the Nestin-progenitors lining the ventricle are negative for PAX3. Right panels are representative of rare sections in which a subset of the Nestin-progenitors lining the ventricle expresses PAX3.

**Additional file 7: Figure S3.** Normal brainstem progenitors isolated from P3 Ntv-a mice were infected with RCAS-Y, RCAS-Pax3, RCAS-PDGF-B, or RCAS-Pax3 + RCAS-PDGF-B. A mRNA from infected cells was isolated and analyzed for PDGF-B expression by RT-PCR. PCR primers for PDGF-B amplify endogenous mouse PDGF-B as well as the human RCAS-PDGF-B. b BrdU incorporation of normal brainstem progenitors from Ntv-a P3 mice infected with the RCAS viruses as indicated below the graph (RCAS-Y vector was used to control for the total amount of virus). Data is represented as fold-change over RCAS-Y.

**Additional file 8: Figure S4.** Ntv-a mice were injected into the cerebral cortex with DF1 cells expressing RCAS-Pax3, RCAS-PDGF-B, or RCAS-PDGF-B + RCAS-Pax3 on P2-4, and monitored for signs and symptoms of brain tumors. a Kaplan-Meier survival curve;  $p = 0.5$ , PDGF-B vs. PDGF-B + Pax3. b Mice from the experiment in (a) were sacrificed at the onset of tumor symptoms, or at 12 weeks in the absence of symptoms, and the brains of all mice were analyzed for the presence of glioma using hematoxylin and eosin (H&E) staining, and their tumors graded as described in Materials and Methods. Shown is the percentage of mice in each group with no tumor, grade II, III, and IV glioma.

**Additional file 9: Figure S5.** Deletion of Pax3 in p53-deficient Brainstem Glioma. Ntv-ap53<sup>fl/fl</sup> mice (Control) and Ntv-ap53<sup>fl/fl</sup>;Pax3<sup>fl/fl</sup> mice (Pax3-KO) were injected with RCAS-PDGF-B + RCAS-Cre into the brainstem at P2-4. Representative Control and Pax3-KO tumors were analyzed for recombination of the Pax3-floxed allele by PCR of gDNA (a) and for PAX3 protein expression by Western blot (b).

**Additional file 10: Table S5.** Differentially expressed genes between human Brainstem Glioma (Brainstem) and Cerebral Cortex Glioma (Cortical) from post-treatment autopsy samples, FDR-adjusted  $p$ -value < 0.05.

**Additional file 11: Table S6.** Differentially expressed genes between human Brainstem Glioma (Brainstem) and Cerebral Cortex Glioma (Cortical) from pre-treatment biopsy samples, FDR-adjusted  $p$ -value < 0.05.

**Additional file 12: Table S7.** Differentially expressed genes between PAX3-High and PAX3-Low Brainstem Glioma post-treatment autopsy samples, FDR-adjusted  $p$ -value < 0.05.

**Additional file 13: Table S8.** Differentially expressed genes between PAX3-High and PAX3-Low Brainstem Glioma pre-treatment biopsy samples, FDR-adjusted  $p$ -value < 0.05.

**Additional file 14: Table S9.** Genetic alterations associated with Pax3 expression in human Brainstem Glioma samples.

#### Competing interest

The authors declare that they have no competing interest.

#### Acknowledgements

We would like to thank Christine Hoeman and Francisco Cordero for mouse PDGF-B;H3.3-K27M;p53-deficient glioma tumors or lysates, Kyle Halvorson for illustration of Figure 7e, Andrew Bendall for the RCAS-Pax3 plasmid, Grigori Enikolopov for Nestin-CFPnuc transgenic mice, Mike Cook and Bin Li for Flow Cytometry, Yasheng Gao for expertise in microscopy, and Dan Wechsler and Robert Wechsler-Reya for critical comments.

#### Financial support

OJB is supported by the Damon Runyon Cancer Research Foundation, U.S. Department of Defense, Rory David Deutsch Foundation, and Pediatric Brain Tumor Foundation; SJB is supported by NIH grant CA096832; SJC is supported by NIH grant HL60714.

#### Author details

<sup>1</sup>Graduate Program in Molecular Cancer Biology, Duke University, Durham, NC, USA. <sup>2</sup>Division of Pediatric Hematology-Oncology, Duke University Medical Center, Durham, NC, USA. <sup>3</sup>Preston Robert Tisch Brain Tumor Center, Duke University Medical Center, Durham, NC, USA. <sup>4</sup>Integrated Biomedical Sciences Program, University of Tennessee Health Science Center, Memphis, TN, USA. <sup>5</sup>Department of Developmental Neurobiology, St. Jude Children's Research Hospital, Memphis, TN 38105, USA. <sup>6</sup>Developmental Biology and Neonatal Medicine Program, HB Wells Center for Pediatric Research, Indiana

University School of Medicine, Indianapolis, IN 46202, USA. <sup>7</sup>Institute for Genome Sciences and Policy, Duke University, Durham, NC, USA.

<sup>8</sup>Department of Pathology, Duke University Medical Center, Durham, NC, USA. <sup>9</sup>Department of Pediatrics, Duke University Medical Center, 450 Research Drive, Durham, NC 27710, USA.

Received: 27 August 2014 Accepted: 27 August 2014

Published online: 21 October 2014

#### References

- Hargrave D, Bartels U, Bouffet E (2006) Diffuse brainstem glioma in children: critical review of clinical trials. *Lancet Oncol* 7(3):241–248, doi:10.1016/s1470-2045(06)70615-5
- Grimm SA, Chamberlain MC (2013) Brainstem Glioma: A Review. *Curr Neurol Neurosci Rep* 13(5): doi:10.1007/s11910-013-0346-3
- Zarghooni M, Bartels U, Lee E, Buczkowicz P, Morrison A, Huang A, Bouffet E, Hawkins C (2010) Whole-Genome Profiling of Pediatric Diffuse Intrinsic Pontine Gliomas Highlights Platelet-Derived Growth Factor Receptor and Poly (ADP-ribose) Polymerase As Potential Therapeutic Targets. *J Clin Oncol* 28(8):1337–1344, doi:10.1200/jco.2009.25.5463
- Paugh BS, Broniscer A, Qu C, Miller CP, Zhang J, Tatevossian RG, Olson JM, Geyer JR, Chi SN, Da Silva NS, Onar-Thomas A, Baker JN, Gajjar A, Ellison DW, Baker SJ (2011) Genome-wide analyses identify recurrent amplifications of receptor tyrosine kinases and cell-cycle regulatory genes in diffuse intrinsic pontine glioma. *J Clin Oncol* 29(30):3999–4006, doi:10.1200/JCO.2011.35.5677
- Puget S, Philippe C, Bax DA, Job B, Varlet P, Junier M-P, Andreiulo F, Carvalho D, Reis R, Guerrini-Rousseau L, Roujeau T, Dessen P, Richon C, Lazar V, Le Teuff G, Sainte-Rose C, Geoerger B, Vassal G, Jones C, Grill J (2012) Mesenchymal Transition and PDGFRA Amplification/Mutation Are Key Distinct Oncogenic Events in Pediatric Diffuse Intrinsic Pontine Gliomas. *PLoS One* 7(2):e30313, doi:10.1371/journal.pone.0030313
- Khuong-Quang DA, Buczkowicz P, Rakopoulos P, Liu XY, Fontebasso AM, Bouffet E, Bartels U, Albrecht S, Schwartzentruber J, Letourneau L, Bourgey M, Bourque G, Montpetit A, Bourret G, Lepage P, Fleming A, Lichter P, Kool M, Von Deimling A, Sturm D, Korshunov A, Faury D, Jones DT, Majewski J, Pfister SM, Jabado N, Hawkins C (2012) K27M mutation in histone H3.3 defines clinically and biologically distinct subgroups of pediatric diffuse intrinsic pontine gliomas. *Acta Neuropathol* 124(3):439–447, doi:10.1007/s00401-012-0998-0
- Schwartzentruber J, Korshunov A, Liu XY, Jones DT, Pfaff E, Jacob K, Sturm D, Fontebasso AM, Quang DA, Tonjes M, Hovestadt V, Albrecht S, Kool M, Nantel A, Konermann C, Lindroth A, Jager N, Rausch T, Ryzhova M, Korbel JO, Hielscher T, Hauser P, Garami M, Klekner A, Bogner L, Ebinger M, Schuhmann MU, Scheuren W, Pekrun A, Fruhwald MC et al (2012) Driver mutations in histone H3.3 and chromatin remodelling genes in paediatric glioblastoma. *Nature* 482(7384):226–231, doi:10.1038/nature10833. nature10833
- Sturm D, Witt H, Hovestadt V, Khuong-Quang D-A, Jones David TW, Konermann C, Pfaff E, Tönjes M, Sill M, Bender S, Kool M, Zapatka M, Becker N, Zucknick M, Hielscher T, Liu X-Y, Fontebasso Adam M, Ryzhova M, Albrecht S, Jacob K, Wolter M, Ebinger M, Schuhmann Martin U, Van Meter T, Frühwald Michael C, Hauch U, Ho KC, Huang A, Radlwimmer B, Niehues T, Von Komorowski G et al (2012) Hotspot Mutations in H3F3A and IDH1 Define Distinct Epigenetic and Biological Subgroups of Glioblastoma. *Cancer Cell* 22(4):425–437, doi:10.1016/j.ccr.2012.08.024
- Wu G, Broniscer A, McEachron TA, Lu C, Paugh BS, Beckwith J, Qu C, Ding L, Huether R, Parker M, Zhang J, Gajjar A, Dyer MA, Mullighan CG, Gilbertson RJ, Mardis ER, Wilson RK, Downing JR, Ellison DW, Baker SJ (2012) Somatic histone H3 alterations in pediatric diffuse intrinsic pontine gliomas and non-brainstem glioblastomas. *Nat Genet* 44(3):251–253, doi:10.1038/ng.1102. ng.1102
- Buczkowicz P, Hoeman C, Rakopoulos P, Pajovic S, Letourneau L, Dzamba M, Morrison A, Lewis P, Bouffet E, Bartels U, Zuccaro J, Agnihotri S, Ryall S, Barszczyk M, Chormenky Y, Bourgey M, Bourque G, Montpetit A, Cordero F, Castelo-Branco P, Mangerel J, Tabori U, Ho KC, Huang A, Taylor KR, Mackay A, Bendel AE, Nazarian J, Fangusaro JR, Karajannis MA et al (2014) Genomic analysis of diffuse intrinsic pontine gliomas identifies three molecular subgroups and recurrent activating ACVR1 mutations. *Nat Genet* 46(5):451–456, doi:10.1038/ng.2936. ng.2936

11. Wu G, Diaz AK, Paugh BS, Rankin SL, Ju B, Li Y, Zhu X, Qu C, Chen X, Zhang J, Easton J, Edmonson M, Ma X, Lu C, Nagahawatte P, Hedlund E, Rusch M, Pounds S, Lin T, Onar-Thomas A, Huether R, Kriwacki R, Parker M, Gupta P, Becksfort J, Wei L, Mulder HL, Boggs K, Vadodaria B, Yergeau D et al (2014) The genomic landscape of diffuse intrinsic pontine glioma and pediatric non-brainstem high-grade glioma. *Nat Genet* 46(5):444–450, doi:10.1038/ng.2938. ng.2938
12. Taylor KR, Mackay A, Truffaux N, Butterfield YS, Morozova O, Philippe C, Castel D, Grasso CS, Vinci M, Carvalho D, Carcaboso AM, De Torres C, Cruz O, Mora J, Entz-Werle N, Ingram WJ, Monje M, Hargrave D, Bullock AN, Puget S, Yip S, Jones C, Grill J (2014) Recurrent activating ACVR1 mutations in diffuse intrinsic pontine glioma. *Nat Genet* 46(5):457–461, doi:10.1038/ng.2925. ng.2925
13. Fontebasso AM, Papillon-Cavanagh S, Schwartzentruber J, Nikbakht H, Gerges N, Fiset PO, Bechet D, Faury D, De Jay N, Ramkissoon LA, Corcoran A, Jones DT, Sturm D, Johann P, Tomita T, Goldman S, Nagib M, Bendel A, Goumnerova L, Bowers DC, Leonard JR, Rubin JB, Alden T, Browd S, Geyer JR, Leary S, Jallo G, Cohen K, Gupta N, Prados MD et al (2014) Recurrent somatic mutations in ACVR1 in pediatric midline high-grade astrocytoma. *Nat Genet* 46(5):462–466, doi:10.1038/ng.2950
14. Zhang L, Chen LH, Wan H, Yang R, Wang Z, Feng J, Yang S, Jones S, Wang S, Zhou W, Zhu H, Killela PJ, Zhang J, Wu Z, Li G, Hao S, Wang Y, Webb JB, Friedman HS, Friedman AH, McLendon RE, He Y, Reitman ZJ, Bigner DD, Yan H (2014) Exome sequencing identifies somatic gain-of-function PPM1D mutations in brainstem gliomas. *Nat Genet* 46(7):726–730, doi:10.1038/ng.2995
15. Sure U, Ruedi D, Tachibana O, Yonekawa Y, Ohgaki H, Kleihues P, Hegi ME (1997) Determination of p53 mutations, EGFR overexpression, and loss of p16 expression in pediatric glioblastomas. *J Neuropathol Exp Neurol* 56(7):782–789
16. Wakabayashi T, Natsume A, Hatano H, Fujii M, Shimato S, Ito M, Ohno M, Ito S, Ogura M, Yoshida J (2009) P16 Promoter Methylation in the Serum as a Basis for the Molecular Diagnosis of Gliomas. *Neurosurgery* 64(3):455–462, doi:10.1227/01.neu.0000340683.19920.e3
17. Saratsis AM, Kambhampati M, Snyder K, Yadavilli S, Devaney JM, Harmon B, Hall J, Raabe EH, An P, Weingart M, Rood BR, Magge SN, MacDonald TJ, Packer RJ, Nazarian J (2014) Comparative multidimensional molecular analyses of pediatric diffuse intrinsic pontine glioma reveals distinct molecular subtypes. *Acta Neuropathol* 127(6):881–895, doi:10.1007/s00401-013-1218-2
18. Lee Da Y, Gianino SM, Gutmann DH (2012) Innate neural stem cell heterogeneity determines the patterning of glioma formation in children. *Cancer Cell* 22(1):131–138, doi:10.1016/j.ccr.2012.05.036
19. Lee DY, Yeh TH, Emmett RJ, White CR, Gutmann DH (2010) Neurofibromatosis-1 regulates neuroglial progenitor proliferation and glial differentiation in a brain region-specific manner. *Genes Dev* 24(20):2317–2329, doi:10.1101/gad.1957110
20. Sharma MK, Mansur DB, Reifenger G, Perry A, Leonard JR, Aldape KD, Albin MG, Emmett RJ, Loeser S, Watson MA, Nagarajan R, Gutmann DH (2007) Distinct Genetic Signatures among Pilocytic Astrocytomas Relate to Their Brain Region Origin. *Cancer Research* 67(3):890–900, doi:10.1158/0008-5472.can-06-0973
21. Robson EJD, He S-J, Eccles MR (2006) A PANorama of PAX genes in cancer and development. *Nature Reviews Cancer* 6(1):52–62, Doi: 10.1038/nrc1778
22. Bang AG, Papalopulu N, Goulding MD, Kintner C (1999) Expression of Pax-3 in the lateral neural plate is dependent on a Wnt-mediated signal from posterior nonaxial mesoderm. *Dev Biol* 212(2):366–380, doi:10.1006/dbio.1999.9319
23. Bang AG, Papalopulu N, Kintner C, Goulding MD (1997) Expression of Pax-3 is initiated in the early neural plate by posteriorizing signals produced by the organizer and by posterior non-axial mesoderm. *Development* 124(10):2075–2085
24. Tanabe Y, Jessell TM (1996) Diversity and pattern in the developing spinal cord. *Science* 274(5290):1115–1123
25. Allen Institute for Brain Science (2013) Allen Developing Mouse Brain Atlas., http://developingmouse.brain-map.org/gene/show/18271
26. Monsoro-Burg A-H, Wang E, Harland R (2005) Msx1 and Pax3 Cooperate to Mediate FGF8 and WNT Signals during Xenopus Neural Crest Induction. *Dev Cell* 8(2):167–178, doi:10.1016/j.devcel.2004.12.017
27. Conway SJ, Bundy J, Chen J, Dickman E, Rogers R, Will BM (2000) Decreased neural crest stem cell expansion is responsible for the conotruncal heart defects within the splotch (Sp(2H))/Pax3 mouse mutant. *Cardiovasc Res* 47(2):314–328
28. Olaopa M, Zhou HM, Snider P, Wang J, Schwartz RJ, Moon AM, Conway SJ (2011) Pax3 is essential for normal cardiac neural crest morphogenesis but is not required during migration nor outflow tract septation. *Dev Biol* 356(2):308–322, doi:10.1016/j.ydbio.2011.05.583
29. Epstein DJ, Vekemans M, Gros P (1991) Splotch (Sp2H), a mutation affecting development of the mouse neural tube, shows a deletion within the paired homeodomain of Pax-3. *Cell* 67(4):767–774
30. Wang XD, Morgan SC, Loeken MR (2011) Pax3 stimulates p53 ubiquitination and degradation independent of transcription. *PLoS One* 6(12):e29379, doi:10.1371/journal.pone.0029379
31. Pani L, Horal M, Loeken MR (2002) Rescue of neural tube defects in Pax-3-deficient embryos by p53 loss of function: implications for Pax-3-dependent development and tumorigenesis. *Genes Dev* 16(6):676–680, doi:10.1101/gad.969302
32. Chen J, Xia L, Wu X, Xu L, Nie D, Shi J, Xu X, Ni L, Ju S, Wu X, Zhu H, Shi W (2012) Clinical Significance and Prognostic Value of PAX3 Expression in Human Glioma. *J Mol Neurosci* 47(1):52–58, doi:10.1007/s12031-011-9677-1
33. Xia L, Huang Q, Nie D, Shi J, Gong M, Wu B, Gong P, Zhao L, Zuo H, Ju S, Chen J, Shi W (2013) PAX3 is overexpressed in human glioblastomas and critically regulates the tumorigenicity of glioma cells. *Brain Research* 1521:68–78, doi:10.1016/j.brainres.2013.05.021
34. Becher OJ, Hambardzumyan D, Walker TR, Helmy K, Nazarian J, Albrecht S, Hiner RL, Gall S, Huse JT, Jabado N, MacDonald TJ, Holland EC (2010) Preclinical Evaluation of Radiation and Perifosine in a Genetically and Histologically Accurate Model of Brainstem Glioma. *Cancer Research* 70(6):2548–2557, doi:10.1158/0008-5472.can-09-2503
35. Barton KL, Misuraca K, Cordero F, Dobrikova E, Min HD, Gromeier M, Kirsch DG, Becher OJ (2013) PD-0332991, a CDK4/6 Inhibitor, Significantly Prolongs Survival in a Genetically Engineered Mouse Model of Brainstem Glioma. *PLoS One* 8(10):e77639, doi:10.1371/journal.pone.0077639
36. Dougherty JD, Fomchenko EI, Akuffo AA, Schmidt E, Helmy KY, Bazzoli E, Brennan CW, Holland EC, Milosevic A (2012) Candidate pathways for promoting differentiation or quiescence of oligodendrocyte progenitor-like cells in glioma. *Cancer Res* 72(18):4856–4868, doi:10.1158/0008-5472
37. Doyle JP, Dougherty JD, Heiman M, Schmidt EF, Stevens TR, Ma G, Bupp S, Shrestha P, Shah RD, Dougherty ML, Gong S, Greengard P, Heintz N (2008) Application of a translational profiling approach for the comparative analysis of CNS cell types. *Cell* 135(4):749–762, doi:10.1016/j.cell.2008.10.029
38. Koushik SV, Chen H, Wang J, Conway SJ (2002) Generation of a conditionalloxP allele of the Pax3 transcription factor that enables selective deletion of the homeodomain. *Genesis* 32(2):114–117, doi:10.1002/gene.10051
39. Encinas JM, Vaahtokari A, Enikolopov G (2006) Fluoxetine targets early progenitor cells in the adult brain. *Proc Natl Acad Sci U S A* 103(21):8233–8238, doi:10.1073/pnas.0601992103
40. Pitter KL, Galban CJ, Galban S, Tehrani OS, Li F, Charles N, Bradbury MS, Becher OJ, Chenevert TL, Rehemtulla A, Ross BD, Holland EC, Hambardzumyan D (2011) Perifosine and CCI 779 co-operate to induce cell death and decrease proliferation in PTEN-intact and PTEN-deficient PDGF-driven murine glioblastoma. *PLoS One* 6(1):e14545, doi:10.1371/journal.pone.0014545
41. Bendall AJ, Ding J, Hu G, Shen MM, Abate-Shen C (1999) Msx1 antagonizes the myogenic activity of Pax3 in migrating limb muscle precursors. *Development* 126(22):4965–4976
42. Lewis PW, Muller MM, Koletsky MS, Cordero F, Lin S, Banaszynski LA, Garcia BA, Muir TW, Becher OJ, Allis CD (2013) Inhibition of PRC2 Activity by a Gain-of-Function H3 Mutation Found in Pediatric Glioblastoma. *Science* 340(6134):857–861, doi:10.1126/science.1232245
43. Dai C, Celestino JC, Okada Y, Louis DN, Fuller GN, Holland EC (2001) PDGF autocrine stimulation dedifferentiates cultured astrocytes and induces oligodendrogliomas and oligoastrocytomas from neural progenitors and astrocytes in vivo. *Genes Dev* 15(15):1913–1925, doi:10.1101/gad.903001
44. Paugh BS, Qu C, Jones C, Liu Z, Adamowicz-Brice M, Zhang J, Bax DA, Coyle B, Barrow J, Hargrave D, Lowe J, Gajjar A, Zhao W, Broniscer A, Ellison DW, Grundy RG, Baker SJ (2010) Integrated Molecular Genetic Profiling of Pediatric High-Grade Gliomas Reveals Key Differences With the Adult Disease. *J Clin Oncol* 28(18):3061–3068, doi:10.1200/jco.2009.26.7252
45. Gautier L, Cope L, Bolstad BM, Irizarry RA (2004) affy-analysis of Affymetrix GeneChip data at the probe level. *Bioinformatics* 20(3):307–315, doi:10.1093/bioinformatics/btg405

46. Gentleman RC, Carey VJ, Bates DM, Bolstad B, Dettling M, Dudoit S, Ellis B, Gautier L, Ge Y, Gentry J, Hornik K, Hothorn T, Huber W, Iacus S, Irizarry R, Leisch F, Li C, Maechler M, Rossini AJ, Sawitzki G, Smith C, Smyth G, Tierney L, Yang JY, Zhang J (2004) Bioconductor: open software development for computational biology and bioinformatics. *Genome Biol* 5(10):R80, doi:10.1186/gb-2004-5-10-r80
47. Gentleman R (2005) Bioinformatics and computational biology solutions using R and Bioconductor. Statistics for biology and health. Springer Science+Business Media, New York
48. Paugh BS, Zhu X, Qu C, Endersby R, Diaz AK, Zhang J, Bax DA, Carvalho D, Reis RM, Onar-Thomas A, Broniscer A, Wetmore C, Jones C, Ellison DW, Baker SJ (2013) Novel oncogenic PDGFRA mutations in pediatric high-grade gliomas. *Cancer Res* 73(20):6219–6229, doi:10.1158/0008-5472
49. Livak KJ, Schmittgen TD (2001) Analysis of relative gene expression data using real-time quantitative PCR and the 2<sup>(-Delta Delta C(T))</sup> Method. *Methods* 25(4):402–408, doi:10.1006/meth.2001.1262
50. Ballester LY, Wang Z, Shandilya S, Miettinen M, Burger PC, Eberhart CG, Rodriguez FJ, Raabe E, Nazarian J, Warren K, Quezada MM (2013) Morphologic characteristics and immunohistochemical profile of diffuse intrinsic pontine gliomas. *Am J Surg Pathol* 37(9):1357–1364, doi:10.1097/PAS.0b013e318294e817
51. Chan KM, Fang D, Gan H, Hashizume R, Yu C, Schroeder M, Gupta N, Mueller S, James CD, Jenkins R, Sarkaria J, Zhang Z (2013) The histone H3K27M mutation in pediatric glioma reprograms H3K27 methylation and gene expression. *Genes Dev* 27(9):985–990, doi:10.1101/gad.217778.113
52. Monje M, Mitra SS, Freret ME, Raveh TB, Kim J, Masek M, Attema JL, Li G, Haddix T, Edwards MSB, Fisher PG, Weissman IL, Rowitch DH, Vogel H, Wong AJ, Beachy PA (2011) Hedgehog-responsive candidate cell of origin for diffuse intrinsic pontine glioma. *Proc Natl Acad Sci* 108(11):4453–4458, doi:10.1073/pnas.1101657108
53. Chen J, McKay RM, Parada LF (2012) Malignant glioma: lessons from genomics, mouse models, and stem cells. *Cell* 149(1):36–47
54. Underwood TJ, Amin J, Lillycrop KA, Blaydes JP (2007) Dissection of the functional interaction between p53 and the embryonic proto-oncoprotein PAX3. *FEBS Letters* 581(30):5831–5835, doi:10.1016/j.febslet.2007.11.056
55. He SJ (2005) Transfection of melanoma cells with antisense PAX3 oligonucleotides additively complements cisplatin-induced cytotoxicity. *Mol Cancer Ther* 4(6):996–1003, Doi: 10.1158/1535-7163.mct-04-0252
56. Scholl FA, Kamarashev J, Murmann OV, Geertsen R, Dummer R, Schafer BW (2001) PAX3 is expressed in human melanomas and contributes to tumor cell survival. *Cancer Res* 61(3):823–826
57. Bernasconi M, Remppis A, Fredericks WJ, Rauscher FJ 3rd, Schafer BW (1996) Induction of apoptosis in rhabdomyosarcoma cells through down-regulation of PAX proteins. *Proc Natl Acad Sci U S A* 93(23):13164–13169

doi:10.1186/s40478-014-0134-6

**Cite this article as:** Misuraca et al.: Pax3 expression enhances PDGF-B-induced brainstem gliomagenesis and characterizes a subset of brainstem glioma. *Acta Neuropathologica Communications* 2014 2:134.

**Submit your next manuscript to BioMed Central and take full advantage of:**

- Convenient online submission
- Thorough peer review
- No space constraints or color figure charges
- Immediate publication on acceptance
- Inclusion in PubMed, CAS, Scopus and Google Scholar
- Research which is freely available for redistribution

Submit your manuscript at  
www.biomedcentral.com/submit

